UNIVERSIDAD NACIONAL AUTÓNOMA DE MÉXICO

PROGRAMA DE MAESTRÍA Y DOCTORADO EN INGENIERÍA
INSTITUTO DE ENERGÍAS RENOVABLES
INGENIERÍA EN ENERGÍA – FUENTES RENOVABLES

ENHANCEMENT OF SOIL MICROBIAL FUEL CELL PERFORMANCE WITH PHOTOACTIVE MATERIALS

TESIS

QUE PARA OPTAR POR EL GRADO DE:
MAESTRO EN INGENIERÍA

PRESENTA:
ING. ALICIA ALEJANDRA MIER JIMÉNEZ

TUTOR PRINCIPAL
DRA. ADRIANA MARGARITA LONGORIA HERNÁNDEZ
CO-TUTOR
DR. JOSEPH SEBASTIAN PATHIYAMATTOM
INSTITUTO DE ENERGÍAS RENOVABLES

TEMIXCO, MORELOS NOVIEMBRE 2020

JURADO ASIGNADO

Presidente: Dr. Pathiyamattom Joseph Sebastian

Secretario: Dra. Arias Lizárraga Dulce María

1er Vocal: Dra. Longoria Hernández Adriana M.

2do Vocal: Dr. Álvarez Gallegos Alberto A.

3er Vocal: Dra. Di Lorenzo Mirella

Lugar o lugares donde se realizó la tesis:
Bath, Inglaterra, Reino Unido
Temixco, Morelos, México

Tutor de tesis:

Adriana Margarita Longoria Hernández

_____

FIRMA

"Life is nothing but an electron looking for a place to rest."
-Nobel prize, Albert Szent-Györgyi

Content

Index of figures

Index of Tables

Acknowledgments – Agradecimientos

Primeramente, agradecer al Consejo Nacional de Ciencia y Tecnología (CONACyT) por la beca No. 2018-000068-02NACF-31828 que me brindó para realizar mis estudios de maestría y por el apoyo de movilidad No. 2019-000016-01NACF-00888 que hizo posible realizar una estancia de investigación en la Universidad de Bath en Inglaterra.

A la Universidad Nacional Autónoma de México (UNAM) es un honor poder graduarme y haber sido parte de la máxima casa de estudios de México.

Al Instituto de Energías Renovables (IER) la institución que me ha formado, y de la cual soy parte. Aquí pude ver con el ejemplo de la excelencia de las personas apasionadas, íntegras y comprometidas con lo que hacen; pude ser testigo de que ponen el corazón y profesionalismo en cada una de las actividades académicas y de integración que se realizan. Esta gran armonía en el cual opera esta institución permitió hacerme crecer, me enseñó que tenía una voz que puede ser escuchada, y a preocuparme y cuestionarme por lo que sucede en el mundo, por esto y mucho más ha sido una parte muy importante en mi formación y sin duda esta etapa marcó un antes y un después tanto académicamente como personalmente, agradezco mucho la oportunidad.

De igual manera, agradezco al proyecto DGAPA-PAPIIT UNAM IN109319 por el apoyo económico de beca, y proporcionar financiamiento para el material y reactivos necesarios para finalizar el proyecto.

Al la Dra. Adriana Margarita Longoria Hernández, mi tutora, por su apoyo incondicional en toda mi travesía académica, por sus valiosos consejos, por ampliar mi perspectiva y por las palabras de aliento cuando fueron necesarias.

Al Dr. Joseph Sebastian Pathiyamatton, mi tutor, por apoyar y creer en la idea que propuse al inicio del curso, gracias por compartir sus experiencias, conocimientos y sobre todo por compartir esa emoción por explorar nuevos proyectos y brindar siempre tutoría y apoyo a sus alumnos de posgrado.

Al Dr. Edgar Borja por abrirme las puertas de su laboratorio en la Fac. de Química de C.U., por sus cátedras impartidas acerca de electrocatalizadores, valoro mucho su tiempo, apoyo y enseñanzas.

A la Dra. Delfeena Eapen por incursionarme y guiarme en la experimentación con plantas y abrirme ese camino maravilloso de la botánica.

Al Dr. Jesús Antonio del Río Portilla y a la Dra. Karla Cedano, por su mentoría, orientación y apoyo en mis inquietudes académicas, de verdad son una gran inspiración para mí.

Quisiera hacer un especial agradecimiento a la Universidad de Bath, en Inglaterra, sobre todo al grupo de Bioenergy, Biofuels and Biosensors y al grupo de Photoelectrochemistry del departamento de Chemical Engineering de dicha universidad, por permitirme usar sus instalaciones, equipos y entrenamientos para poder realizar completamente el trabajo experimental de esta tesis. También, agradezco mucho a los investigadores y estudiantes del Departamento de Chemical Engineering por los conocimientos, experiencias y consejos, a los cuales nombro a continuación:

Un especial agradecimiento a la Dra. Mirella di Lorenzo, líder del grupo de Biosensors, Bioenergy and Biofuels, por abrirme sus puertas a su laboratorio, por creer en mí y darme esta magnífica oportunidad, por su generosidad y apoyo a lo largo de toda mi estancia. A los investigadores y estudiantes de este magnífico grupo de investigación: Elena, Bongkyu, Carla, Barbara, Jakub y Adil por sus consejos, mentoría y sugerencias a lo largo de toda mi estancia y también por las experiencias compartidas.

También otorgo un especial agradecimiento al Dr. Salvador Eslava y a sus estudiantes: Miriam, Emma, Santosh y Ria, por abrirme también sus puertas a sus laboratorios tanto en La Universidad de Bath como en el Imperial College of London, por su amabilidad, y por su disposición en ayudarme y atender dudas, incluso en la distancia. También, por sus valiosas enseñanzas y consejos en fotoelectroquímica y síntesis de materiales.

A la comunidad mexicana de la Universidad de Bath, a los investigadores y a la comunidad estudiantil de la que fui parte: a Benjamín, Giove, Ana, Sanmoy, Umir, Barush, Carlos, Karina, Isaac y Vesna, así como a los integrantes de la banda “El Ganso”: Bernardo y Andrés, por las experiencias compartidas durante esos 6 maravillosos meses por tierras inglesas.

De igual manera, agradezco el apoyo incondicional de mi familia que sin ellos no pudiera haber llegado hasta aquí, a mi mamá y mis hermanos: Gerardo, Yrma y sus respectivas familias, a mi tío Hipólito Mier y a los míos que me han apoyado en la distancia. Y agradezco especialmente a mi padre, Gerónimo Mier Castillo, que me dio el coraje necesario para poder enfrentarme a mí misma, y como consecuencia emprender esta aventura.

A mis compañeros del IER, que se convirtieron en familia, siempre los recordaré con el corazón. A mis amigos de siempre: Rafa, Moni, Seijel, Karí, Olga, Pepe, Norma, Paola, y Sam los cuales me hacen saber que siempre tengo a alguien con quien contar y tener a dónde regresar. Y a una mención especial: Carmen Lizárraga, por su ayuda, que sin ella no hubiera comenzado esta aventura. Agradezco también a la gente que se quedó, y a los que dejaron marca, pero emprendieron otro camino.

Esto ha sido toda una aventura, además de académica, me dio la oportunidad de poder explorar otros horizontes e ideas que se sintetizan en solo 80 páginas académicas y muchos de ellos aún se quedan por explorar. El aprendizaje personal que me llevo de esta etapa es muchísimo más profundo y significativo para mí.

Infinitas gracias a esta experiencia a esta aventura, porque aquí me pude dar cuenta de lo que la vida trata y de lo que puedo ser capaz o al menos de tener la oportunidad de explorarlo. Sobre todo, de esta etapa aprendí que la infinita curiosidad, la disposición, el compromiso y el auténtico interés por aprender y resolver un problema pueden conducirte a lugares, personas y experiencias increíbles.

Con esta gran experiencia, me recuerdo a mí misma nunca dejar de ser curiosa, comprometida y, sobre todo, valiente.

A mi padre,

Gerónimo Mier Castillo

Abstract

One of the biggest challenges of this century is the energetic transition that clean energy satisfices the actual demand of energy for future generations. The bioelectrochemical systems transform the biomass into electricity through the electrochemical reactions present in bacteria metabolism. The principal limiting factor of these devices is the reaction kinetics carried out in the cathode surface.

This work is focused in the application of photoelectrocatalytic materials such as Cu_2O and $LaFeO_3$ was synthetized by solvothermal and spin-coating method, respectively. Both materials were characterized by high resolution optical microscope, SEM and XRD to evaluate the surface morphology and structure and Linear Sweep Voltametry (LSV) to evaluate the photoelectrochemical behaviour.

The morphological characterization showed a tetrahedral shape in Cu_2O nanoparticles and a uniform $LaFeO_3$ film. The results of XRD shows that the predominant plane was (111) in Cu_2O films. The electrochemical characterization showed that Cu_2O is very active in the photocurrent production, and the photoactivity of $LaFeO_3$ starts at more positive potentials compared with Cu_2O. However, $LaFeO_3$ presents one magnitude unit lower in the current density production. Additionally, the added Nafion layer on the Cu_2O samples increases the current production. On the other hand, three Soil Microbial Fuel Cells systems (SMFC) were constructed and characterized. Afterward, cathode was replaced by the semiconductor films Cu_2O, Cu_2O with a Nafion layer, and $LaFeO_3$ and discharge test were carried out for each system.

The polarization test results presented a considerably increase in the V_{OC} of each system Cu_2O and Cu_2O + Nafion. In this last system, an increase on I_{SC} was also observed in light and dark conditions. $LaFeO_3$ presents an increment of almost 216% of V_{OC} and I_{SC} under light conditions. This can be due to the early photovoltage production in the $LaFeO_3$ that catalyses the cathodic reactions. However, the power production performance is poor compared to other studies due a high ohmic losses present in the systems. Despite that, the activation losses were considerable reduced when the photocathodes were implemented.

This work presents an alternative to enhance Soil Microbial Fuel Cells performance for its potential applications and scale up.

Resumen

Uno de los retos para este nuevo siglo es la transición energética a energía limpia que satisfaga la demanda actual y creciente para las generaciones futuras. Los sistemas bioelectroquímicos son sistemas que transforman la biomasa en energía eléctrica a través de las reacciones electroquímicas presentes en el metabolismo de las bacterias. El principal factor limitante de estos dispositivos es la cinética de reacción llevada a cabo en el cátodo.

Este trabajo se centra en la aplicación de cátodos de materiales fotoelectrocatalíticos, Cu_2O y $LaFeO_3$, para mejorar el desempeño de una Celda de Combustible Microbiana a Base de suelo, que fueron sintetizados por el método solvotermal y spin-coating, respectivamente. Ambos materiales fueron caracterizados por microscopía óptica de alta resolución SEM, y DRX y fotoelectroquímicamente usando la técnica de voltamperometría de barrido lineal.

Las caracterizaciones morfológicas mostraron una forma tetraédrica en las partículas de Cu_2O y una muestra uniforme en cuanto a las películas de $LaFeO_3$. Los resultados de DRX mostraron que el plano predominante fue el (111) en las películas de Cu_2O. Las caracterizaciones electroquímicas mostraron que el Cu_2O es muy activo en la producción de fotocorriente y que la fotoactividad del $LaFeO_3$ comienza a voltajes más positivos que la fotoactividad del Cu_2O, sin embargo, presenta una unidad de magnitud menor en densidad corriente. Al añadir una capa de Nafion a las películas de Cu_xO, se observa un incremento en la corriente. Posteriormente, tres sistemas de celdas de combustible microbianas a base de suelo fueron construidas y caracterizadas. El cátodo fue reemplazado por las películas de Cu_2O, Cu_2O con una capa de Nafion y $LaFeO_3$ y se realizó una prueba de descarga para cada sistema.

Los resultados de la curva de polarización y curvas de potencia presentaron un aumento considerable en el V_{OC} de cada sistema de Cu_2O y Cu_2O + Nafion, en este último se observó también un aumento en la I_{SC} tanto en condiciones de luz como en oscuridad. En el caso del $LaFeO_3$, presentó un aumento del 216% del V_{OC} y I_{SC} en condiciones de iluminación. Esto se debe que la fotoactividad comienza a potenciales más positivos en el $LaFeO_3$, catalizando las reacciones que se llevan a cabo en el cátodo.

Este trabajo presenta una alternativa para mejorar el desempeño de las Celdas de Combustible Microbianas a base de suelo para su posible escalamiento y aplicación.

Chapter 1 - Introduction

Since the Industrial Revolution, fossil fuel demand has dominated the energy market (see Figure 1). However, they are finite resources, with population growing year by year, these resources are unsustainable to cover the energy demand in the long term.

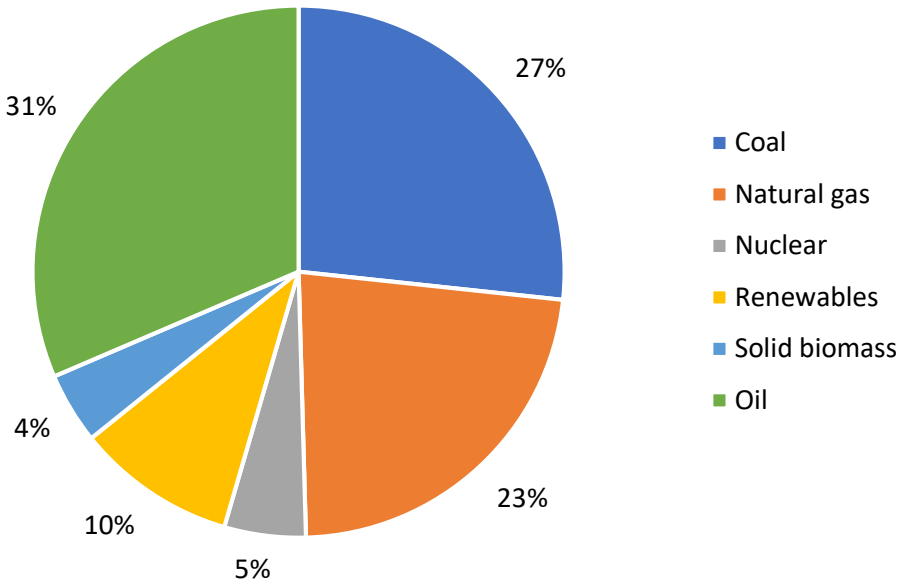

Figure 1. Total primary energy supply by type in 2018 (IEA, 2019)

Additionally, climate change is a major issue and it is related to fossil fuels usage: the over usage of these carbon resources is causing the increase of the CO_2 and other greenhouse gases in the atmosphere, warming the planet and negatively affecting our ecosystems, natural renewable resources and human health as consequence.

One of the most significant environmental and human challenges is the energy transition to renewable energy resources to satisfy the energy demand with a minimal environmental impact. Nowadays, 1 of 7 people have a limit or null access to electricity, most of them live in rural areas in developing countries. On the other hand, energy is the main contributor to climate change, producing 60% of greenhouse gases. For this reason, one of the Sustainable Development Goals of the United Nations is Goal 7: "Affordable and clean energy". To achieve this ambition, the development of technology to use more sustainable energy sources such as solar, wind, water as hydro energy, geothermal and biomass energy, must be done. "Expanding infrastructure and upgrading technology to provide clean and more efficient energy in all countries will encourage growth and help the environment" (*Sustainable Development Goals*, 2020).

Biomass is one of the most potentially attractive sources of energy and is the most social impact improving energy source. This energy could be expressed in several forms, the most common is the direct combustion of biomass; also, biofuels production through fermentation (bioethanol), gasification (methane and other biogases production), pyrolysis, and transesterification processes (Zabaniotou, 2018).

Other advanced processes to transform the biomass are developing on this time, to make the biomass fuel energy more affordable and efficient. One of the most conceptually attractive technologies due to its potential to provide low-cost electricity production is the Microbial Fuel Cell device (Venkata Mohan et al., 2014). This work will be focused on this bioelectrochemical technology.

Overview of Bioelectrochemical Systems

The history of generating electricity from bacteria dates back to 1911 when M.C Potter discovered and demonstrated electricity generation by *Escherichia coli*, by inserting a platinum electrode in an *E. coli* suspension (Potter, 1915). Some sporadic work was done through the 20th century but the technology has started to achieve attention from the scientist until the final quarter-century, when the technology was re-discovered to explore its potential, especially at the decade of 1990 (Harnisch & Rabaey, 2015).

The most typical Bioelectrochemical System (BES) is the Microbial Fuel Cell (MFC) system whose principal function is to convert the chemical energy of a substrate, it could be wastewater, soil, or another medium which has a great content of organic material, into electricity by a chain of redox reactions present in microbe's metabolism. The organic matter is oxidised by microorganisms at the anode, this process generates electrons which pass through an external circuit to the cathode, this electron movement results in an electrical current (Gul & Ahmad, 2019).

This kind of bioelectrochemical reactions offers to BES technology another way to see the feedstock, on a bigger potential way and enhance the availability of the technology because where there is organic matter, a Microbial Fuel Cell device could be applied. This characteristic gives to BES technology potential to be implemented in many scenarios where there is no access to electricity (Gul & Ahmad, 2019).

Principles on Microbial fuel cells

Microbial fuel cells components and design

The definition of a Microbial Fuel Cell is a bioelectrochemical device that uses the natural metabolism of microbes to produce electrical energy (Dziegielowski, 2018). This system consists of

two electrodes: an anode and a cathode separated in two chambers by a proton exchange membrane as is shown in the Figure 2. Each component has its specific function in the system: in the anodic chamber the organic matter is oxidized by bacteria metabolism present in the substrate, microorganisms can transfer electrons from its membrane to the species of the environment to reduce electron acceptor species (such as oxygen). Instead of transfering electrons to these species, they can transfer it to a conductive material which is called the anode. The anode is connected to a wire and this to an external resistor. In the other side of the MFC the cathode is found, in this compartment is where the electrons from the anodic chamber are transferred to the elements present in the environment, most typically to the Oxygen element, through electro-catalysed reduction reaction to form water (Reaction 2) or other reduced species, depending on which components are present in the cathode chamber. The passing of electrons from the anode to the cathode by a conductive wire produces a direct electric current (Gul & Ahmad, 2019; Palanisamy et al., 2019; Venkata Mohan et al., 2014). As in a fuel cell, the overall voltage is produced because the electrode potential of each half cell reactions (Reaction 3) (Venkata Mohan et al., 2014):

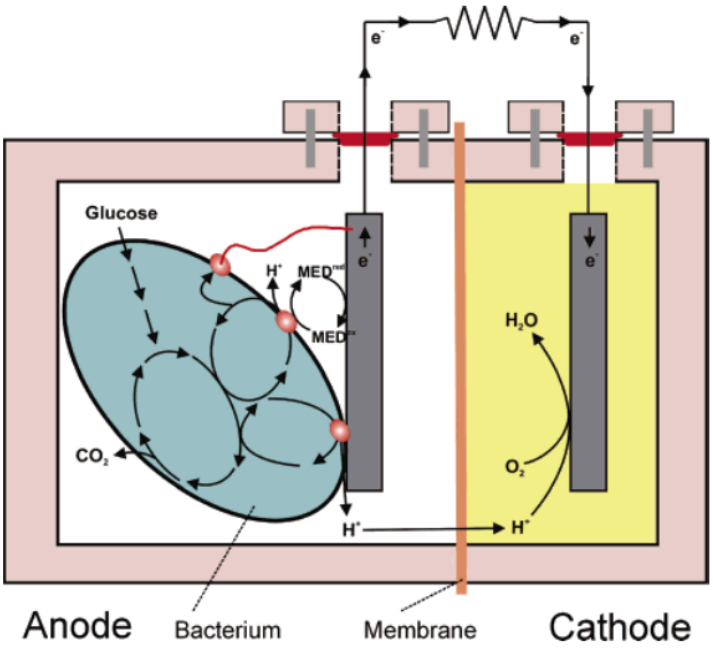

Figure 2. Microbial Fuel Cell (B. E. Logan et al., 2006)

Anodic reaction:

$$C_6H_{12}O_6 + 6H_2O \rightarrow 6CO_2 + 24H^+ + 24e^- \quad (1)$$

Cathodic reaction:

$$O_2 + 4H^+ + 4e^- \rightarrow 2H_2O \quad (2)$$

Overall reaction:

$$C_6H_{12}O_6 + 6H_2O + 6O_2 \rightarrow 6CO_2 + 12H_2O \quad (3)$$

Microbial Fuel Cell technology is still in developing stages, but it shows great potential due to many operational and functional advantages and simplicity, but also provides carbon-neutral renewable energy that can be harvested from organic matter, with no harmful by-products. The technology could have a simpler and more cost-effective design compared to the other BES and can be operated at any location in the world.

Microbes and substrates

The most important resource in a Microbial Fuel Cell are microbes, which are catalysts for oxidation of organic matter and where the production of electrons occur. The electrogenesis is directly related to the metabolic pathways of bacteria, and in some cases, the produced electrons are transferred without an exogenous electron mediator. The electroactive bacteria follow similar metabolic routes, the most studied microbes are members of *Clostridium*, *Geobacter*, *Shewanella* and *Pseudomonas* genera (Palanisamy et al., 2019). The electron transfer mechanism is the ability of the microorganism to transfer electrons, and there are three different mechanisms to do that, as shown in Figure 3 (Venkata Mohan et al., 2014):

i) Direct electron transfer. This involves the transfer of electrons by pili outgrowth.

ii) By redox-active proteins. These active proteins are present on the outer membrane of the microorganism and they are named c-type cytochrome membrane-bound proteins.

iii) Mediated electron transfer (MET). This mechanism uses mediated electron shuttles, additional molecules which are oxidized and reduced where the electrons are transported via metabolites or redox mediators. This mechanism is also called Indirect Electron Transfer.

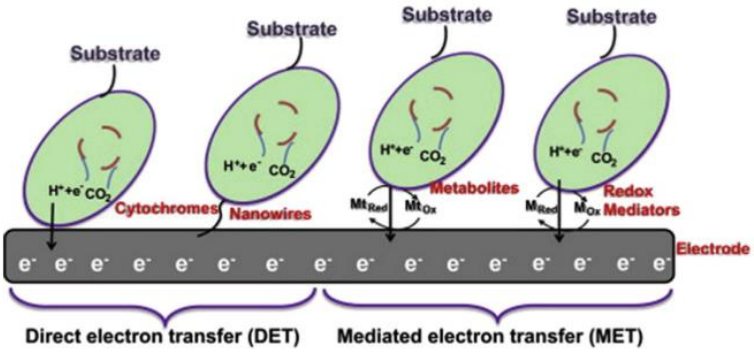

Figure 3. Electron transfer mechanism (Venkata Mohan et al., 2014)

The organic substrates which are biomass-rich and are used to feed the microorganism can be derived from agricultural, municipal and industrial wastes. Another advantage of MFC is that it is not limited by the Carnot cycle because of the direct conversion of chemical energy to electricity without partial heat losses. It can provide high energy conversion efficiency, up to 70% compared to the typical chemical fuel cells. The MFC performance efficiency and functionality depends on the substrates available for microbial metabolism and the presence of other electrons acceptors.

Anode

One of the most significant components of the Microbial Fuel cells is the anode which is responsible to collect the flow of electrons produced by the electrochemical reactions from bacteria metabolism (Palanisamy et al., 2019). The properties which influence the MFC performance are their effect on bacterial adhesion and the effectiveness of the interfacial electron movement from microbes to electrodes and from the electrodes to the substrate. The increase of surface area for the formation of a specific biofilm and the interactions of the microbe-electrode-electrolyte system are anode properties related to the electron transfer mechanism. Metabolic rates of the bacteria are enhanced by the anode material because the anode provides another anaerobic terminal electron acceptor for oxidizing organic matter (Palanisamy et al., 2019).

Since the beginning of the technology, carbon was the most prevalent material used as the anode, and its variances: graphite, carbon nanotubes, brushes, rods and plates (Gul & Ahmad, 2019; Palanisamy et al., 2019). Metal electrodes as molybdenum, stainless steel, silver, nickel, titanium, and copper have been recently used as anodes because the material would have a 3D structure that can provide a large reactive surface area which enhances molecular diffusion. Nevertheless, these materials present fewer adhesion properties and lower electron transfer efficiencies compared to carbon materials. Alternatively, the implementation of nanostructured materials and the modification of the conventional materials have been identified as potentially useful, materials such as carbon black, carbon nanotubes, porous carbon, graphene, and polyaniline or other composite materials could reduce the ohmic losses and enhance bacterial cell adhesion for increasing the efficiency, influenced by the modifications of anodes with metals of their oxide-based nanocomposites (Gul & Ahmad, 2019; Palanisamy et al., 2019).

However, carbon-based anode materials are the most promising candidates for MFC by their cost-effectiveness, greater electricity potential, higher surface area and large pore volume and stability.

Cathode

The cathode is the place where the electrons generated at the anode are collected, which are conducted by an external wire and is where the oxygen reduction reaction (ORR) takes place. The high

redox potential of the cathode is desirable to catch the protons and to make a high potential difference concerning the anode. The electron transfer occurs from the electrode to the species present in the catholyte, usually, the electron acceptor is the oxygen, for that reason is necessary a proper oxygen flux near to the cathode to guarantee the efficiency of electron flux (B. E. Logan et al., 2006). It is crucial to improve cathodic activity with the presence of a catalyst for the ORR reaction. In this way, the platinum is the preferred cathode material, due to its high surface area and catalytic activity. However, due to their very high cost and non-biocompatibility, platinum electrodes are not viable for scalable applications and commercialization of the technology. Some MFC researchers have been given some catalyst alternatives. An effective catalyst will reduce the activation energy on the cathode in an MFC, and it could be biotic an abiotic catalyst. One of the most important factors in MFC is to increase the cathodic kinetics (Rismani-Yazdi et al., 2008). This topic will be discussed later.

Membrane

The membrane function is mediate the ion transport, and separate positive and negative electrodes, also prevents cross between anode and cathode, especially by CO_2 and O_2 flow. The membrane material is selected considering resistance, substrate loss, biofouling and oxygen diffusion. There are some membrane materials such as perfluorinated polymer membranes and composite materials. However, due to high proton conductivity, Nafion® which was developed by DuPont™ in 1970s decade, is the most used commercial membrane in fuel cell technology. However, high cost and non-biocompatibility are the biggest issues of these materials. Alternatively, there are many strategies to reduce the cost of this membranes and to improve its proton exchange efficiency, for example, the addition of some metallic oxides such as SiO_2, TiO_2, ZrO_2 to a Nafion® membrane to improve their efficiency are reported. Recently, novel cross-linked semi-fluorinated sulfonated polytriazole cross-linked with Polyynyl alcohol membrane was synthesised, the crosslinking property resulted in more water absorption, a dimensional change and increased oxidative stability of the MFC. On the other hand, Nafion® replacements have been developed, namely, sulfonated polymer materials (Gul & Ahmad, 2019; Palanisamy et al., 2019).

Additionally, another ion exchanger as ceramics and different fibres have been considered for MFC applications. For instance, cotton fabric-based membrane coated with polyvinyl acetate-grafted-polyvinylidene fluoride (PVAc-g-PVDF) to use in a wastewater purification process and a PVA hydrogel with a light extended clay addition, where it was demonstrated that the clay addition improves the proton conductivity and longevity of the MFC (Palanisamy et al., 2019).

Single-chamber membrane-less systems were also suggested as an alternative solution to the membrane high costs. However, the oxygen diffusion at the anode as well as the need to keep the

electrodes a certain distance apart, affecting the performance of the fuel cell (Gul & Ahmad, 2019). More research is still needed for optimizing the membrane-less MFC design to achieve feasibility in these systems.

Activation losses in a microbial fuel cell

MFC operation has many-electron losses during the electron transfer process from the biocatalyst to anode, hence when electrons reach the cathode the conversion efficiency lowersFigure 5). The generated electrons from the metabolic substrate need to overcome many barriers to reach firstly the anode and then the cathode. During these processes, many possibilities exist for the systems to have electron losses, and due to their possible neutralization, these are accepted by other electronegative species present in the substrate, for that reason a quenching of electrons exists either. Electron transport mechanism is influenced by internal resistances. At lower current densities these kinds of losses are considered crucial. The electron transport is governed by diverse factors: biocatalyst nature, cell design, MFC components, operational conditions and the nature of the anolyte or catholyte. The influence of internal and external resistances can be studied by Tafel plots, and polarization profiles, from this study it is possible to derivate kinetic parameters to analyse and characterise the performance (Larminie et al., 2013; Venkata Mohan et al., 2014).

Ideally, in the studies mentioned above, the power curve is parabolic in shape as the power output reaches a peak and drops down to the base (Figure 4). The resistance where the power peak is located is where the cell operates in optimum conditions and it is called the Cell Design Point (CDP) (Larminie et al., 2013).

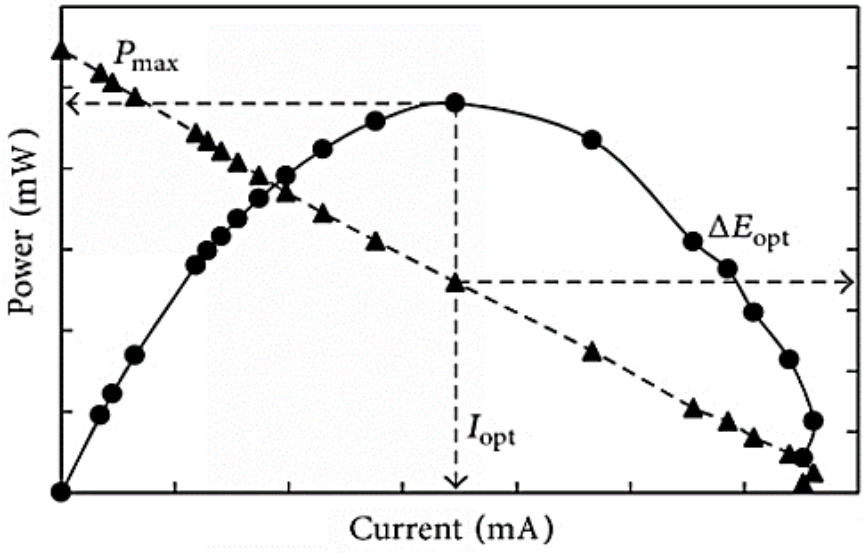

Figure 4. Power curve + Polarization curve (Dziegielowski, 2018)

The voltage curve ideally has an S-shape where the early region describes concentration losses. Each stage represents and describes activation overpotentials (Rismani-Yazdi et al., 2008; Venkata Mohan et al., 2014):

- *Initial region - activation overpotential:* this region depicts the internal losses of the systems, the electron flow obstructions from the biocatalyst to the anode. This is caused by the energy barrier that the biological reactants must cross to form products.
- *Middle region - Ohmic losses:* This region is caused by the electrical resistance of the electrodes and external circuit, and the interfaces electron-electrolyte and electrolyte-membrane. These losses appear when the optimum voltage and current are achieved. Controlling these ohmic losses could help to achieve higher power densities by using highly conducted electrode materials, increasing the electrode conductivity and minimizing these losses.
- *Terminal region - concentration losses:* This is caused when the oxidative force of the anode becomes faster and the products of the oxidation reactions cannot be efficiently carried to the cathode. This is important at higher current densities when the MFC becomes unstable. Thick and nonconductive biofilms create a resistance in the anode surface. However, biofilm is still electrochemically active and has efficient electron transfer.

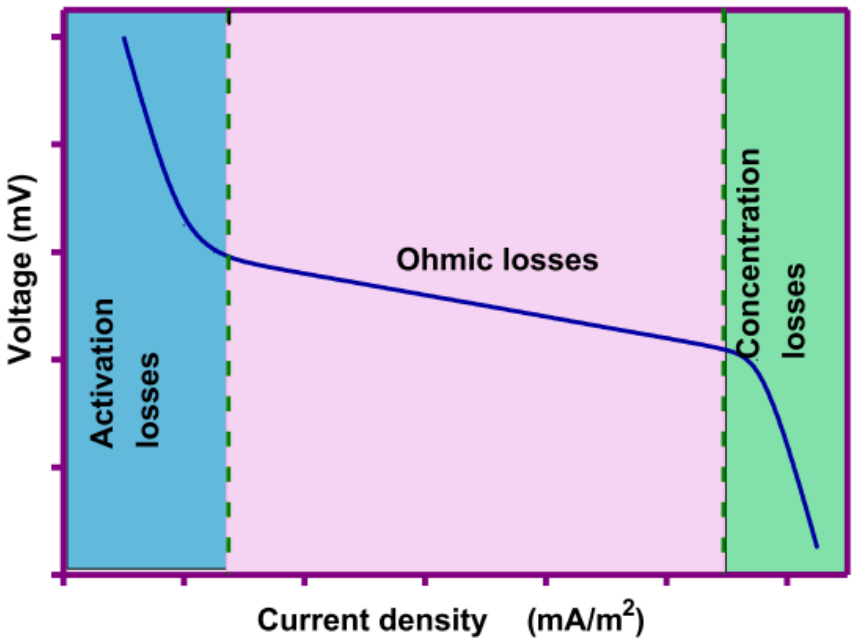

Figure 5. Polarization Curve (Venkata Mohan et al., 2014)

Cathode limitation and cathode activation losses

As in chemical and biological fuel cells, the cathode losses dominate the fuel cell behaviour. These losses also have the three components mentioned before.

The current production at the cathode depends on the kinetics of the reduction reaction at the electrode, which is limited by activation energy that prevents oxidant conversion to its reduced forms. In a fuel cell, when the current gets down, part of the cathodic potential is lost to reach and overcome the activation barrier. This phenomenon is called cathodic activation loss $(\eta_{act})_{cathode}$, or activation overpotential. When a high current is generated from an MFC, activation energy increases and results in a lower cell potential. The cathode activation magnitude depends on reduction kinetics. Some strategies to decrease the activation barrier is increasing the interface interaction area, increase temperature or the oxidant concentration (Rismani-Yazdi et al., 2008).

As it was mentioned before, the ORR is the most common cathodic reaction in MFC, and one of the causes of a high reduction overpotential is the slow rate of oxygen reduction on the surface of the electrodes. Some strategies were developed to optimizing these operations as the use of a mediator, modification with catalysts, optimizing operational conditions within the cathodic compartment (Palanisamy et al., 2019; Rismani-Yazdi et al., 2008) etc.

Enhancing of cathode activity

Catalyst

The use of a catalyst in a cathode surface can lower the cathodic overpotential and increase the current output because it considerably decreases the activation energy barrier and improve the ORR kinetics. Different chemical and biological catalyst have been tested in efforts to improve MFC performance.

Photoactive materials and photocatalysis

Photocatalysis was discovered by Fujishima and Honda in 1972 (Fujishima & Honda, 1972). The researchers proved they were very effective in the degradation of pollutants with very fine results. In comparison to others redox processes, the advantages of photocatalysis can be used to degrade dyes and chemicals completely and are very helpful in the degradation of very stable compounds compared to other processes, also they can work efficiently at room temperature and pressure conditions, and oxygen supply is not necessary. Photocatalysis is a cheap process compared to the other redox processes. Many photocatalysis processes have been studied, where the most studied and considered model in the field is the TiO_2, but also other oxides have been studied before, as ZnO, WO_3, Fe_2O_3, CdSe and $SrTiO_3$ (Zhang et al., 2018). An ideal photocatalyst should have these properties:

- Must be active under UV, visible light or solar light radiation.
- Chemical and biological stability.
- Stability against photo-corrosion.
- Nontoxic and easy availability.

Mechanisms of Photocatalytic Redox reactions

The chemical reactions in a semiconductor occur when the material is capable to transfer electrons from valance band to conduction band. As the number of orbitals (N) in the HOMO and LUMO increases, the energy to transport electrons from the valence band to the conduction band decrease.

The photocatalytic mechanism is quite complex but the principle is the same: under light radiation conditions where the energy radiation is equal or higher than the bandgap of the semiconductor used as a photocatalyst, the electrons are excited from the valence band to the conduction band, leaving holes in valence bands, which are the electron unoccupied spaces in that band, as is shown in Equation (4).

$$Semiconductor + hv \rightarrow e^- + h^+ \quad (4)$$

The photo-generated electrons and holes can recombine by releasing the heat between 10 nanoseconds and 100 nanoseconds (Equation (5)). This recombination causes the low quantum efficiency of the photocatalyst.

$$e^- + h^+ \rightarrow heat \quad (5)$$

Recombination of photogenerated electrons and holes occurs in the bulk of the catalyst samples. This process can be reduced significantly if these charge-carriers are separated by the addition of a charge-carrier acceptor or incorporation of some trap sites on the surface or surface absorbents. If we provide enough time to the holes and electrons before they recombine these can migrate to the catalyst surface and do a charge transfer mechanism and be able to initiate a redox reaction by surface species interaction (Zhang et al., 2018).

Photocatalyst for Microbial Fuel Cells

*There are some works in the literature about light supported MFC systems, where it shows their power increases with illumination. But these works represents only less of 2% of the whole published knowledge of the microbial fuel cells systems (Fischer, 2018).

The Light-supported MFC systems can have different configurations (Fischer, 2018):

- Photo-bio-anode MFC systems: This configuration combines an electroactive bacteria growth over a photoactive material, generally a semiconductor, at the anode chamber. When this semiconductor was irradiated a charge separation happens inside of the electronic configuration of the material, the holes formed at the cathode compartment enhance the excitation of the electroactive bacteria to produce more electricity when the capacity of the biofilm to supply electrons is a potential limitation. This is because improving biofilm thickness by enhancing metabolic respiration, caused by illumination, accelerates electron transfer mechanism from microbes to electrodes, it is comparable as electro-stimulation using a potentiostat. The most studied electrode for these applications has been TiO_2.
- Photosynthetic MFC systems. This can be divided into two uses of microalgae in a MFC for biomass production, and for generation of electrons. In the first one, the microalgae biomass production is used as a good substrate for electroactive bacteria at the anode chamber. Additionally, microalgae produce oxygen and it could be a replacement to the oxygen bubbling at the cathode to guarantee the access of this electronic acceptor. The second one, microalgae use special species which become part of the biofilm formation. Electrogenic microalgae are used at the anode and are electron donators like any other electrogenic bacteria.
- Photocathode: This configuration adds a semiconductor photocatalyst as the cathode in MFC and operates under light irradiation conditions. The charge carriers obtained by the interaction of the semiconductor by light will increase the presence of electrons and, enhance the electron transfer mechanism to reduce the present species at the cathode chamber.

Photocathodes for microbial fuel cells.

This section is dedicated to critically explore the background about photo-bio electrochemical systems which uses semiconductors materials and composites as cathode replacement in MFCs to identify the materials, outputs and diverse configuration and applications of these innovative systems. Table 1 resumes the studies and results that have been carrying out.

The first study where in which photoactive material was used was carried out by Li et al. (Yan Li et al., 2009) in 2009. The study was focused in using a coated solid graphite electrode with rutile, that is a crystal phase of TiO_2 which is an n-type semiconductor, in a double chamber microbial fuel cell to reduce Cr (VI) with simultaneous power generation. The results showed the Cr (VI) reduction was 1.6X times faster under light conditions than in dark conditions. This firstly opens a new alternative to replace a noble metal catalyst. Lu et al. (Lu et al., 2010) used the same rutile coated cathode to evaluate the electricity generation of a double chamber MFC, finding an increase of 223% vs a plain graphite cathode and 33% lower than a Pt cathode, which power peak under light conditions was 12.03 W/m^3. This study also suggests some electron transfer mechanisms on cathode interphase and overall reaction kinetics explaining how semiconductor carriers and activation energies can work. The next studies about rutile or TiO_2-based photocathode-MFC system were applied on dye reductions (Ding et al., 2010), where a decrease on internal resistances of MFC system was found, from 1378 ohms to 443 ohms under dark and light conditions, respectively. Hydrogen generation was another application where TiO_2 nanoarrays were used as photocathode to overcome the thermodynamic barrier for hydrogen production (Chen et al., 2013) from acetate using a 10 kΩ external resistance and obtaining a power peak of 6 mW/m^2, this was the first reference of a novel potential photocathode-MFC potential application.

Wang et. al. (S. Wang et al., 2014) reported a dual chamber microbial fuel cell which uses a $CuInS_2$ flower-like photocathode to produce electricity, obtaining 0.108 mW/cm^2 and a current density of 0.62 mA/cm^2 as a maximum power peak under light conditions, which was comparable to Pt coated carbon electrode, this work also suggests a reaction mechanism of charge carriers separation and cathode electrode transfer for ORR.

Some hybrid systems were also reported for dye degradation, and hydrogen production, those systems consist in two MFC systems in separate chambers, one of the systems have one or two photoelectrodes, the cathode and anode of both chambers are connected one by one, it means that the anode of bio-photoelectrochemical (BPEC) system is connected to MFC cathode and MFC anode is connected to the photocathode of BPEC where the hydrogen reduction carries out; Wan et al. (Wan et al., 2015) report a 0.68 A/m^2 and a 1.35 mL/h of hydrogen production using the described hybrid

system under light conditions. Other use of hybrid systems for $ABRX_3$ is the decolourization and intermediate products degradation with a combination of an MFC and a photoelectrochemical (PEC) system, where the synergetic effect also can measure the effect of light in the system (Long et al., 2017).

On the other hand, photoelectrochemical nanoparticles were used as electron transfer mediator in the cathode chamber, Jiang et al. (Jiang et al., 2016) reported methylene blue and tetracycline destruction for textile wastewater treatment using Fe^0/TiO_2 nanoparticles achieved a 94% of complex compounds removal under visible light illumination.

Photocatalytic composite membrane coated with CoA_2O_4, where A = Ni, Fe, Co and Zn, and polyvinylidene fluoride (PVDF) with carbon fibre were used to enhance ORR activity in an MFC system for tetracycline hydrochloride removal (Yihua Li et al., 2017a). The best of these composites was $CoFe_2O_4$ with a modified conductivity PVDF membrane which was the electrode that achieves the highest power density peak of 942 mW/m^3.

Other parameters were also explored in the case of the pH effect in this Cr(VI) removal study (Han et al., 2018) where was found that at lower pH value enhanced the heavy metal wastewater treatment, following the pseudo-first-order reaction analysis.

Furthermore, TiO_2 was the first material applied and the most studied in PEC-MFC systems, but the TiO_2 only absorbs light in the UV region. Exploration of other material which absorbs under visible region has been carried out like doped materials or other p-type semiconductors. Bhowmick et. al (Bhowmick et al., 2018) doped TiO_2 with Bismuth to decrease TiO_2 bandgap. From 3.26 eV of pure TiO_2 to 2.8 eV. Another case of an hybrid system was constructed using a MoS_2/TiO_2 nanotube electrode prepared by electrostatic functionalization which bandgap was 2.9 eV (Zeng et al., 2019). Another sophisticated nanoarrays as nanowires (Guo et al., 2019; Han et al., 2018) nanorods (Li, Xihuan), or hybrid semiconductor oxides (Tahir, 2019) were proved.

Cu_2O

Cuprous oxide (Cu_2O) is a p-type semiconductor with a 2.0-2.2 eV that has shown great potential for photocatalysis. Cu_2O can be synthesized by low-cost methods like hydrothermal, solvothermal or electrodeposition. This material demonstrates high efficiency, low toxicity, and environmental acceptability. Also, Cu_2O has the advantage that is reactive at visible light region compared to other conventional materials, such TiO_2 that is photoreactive at UV-light due to its wide bandgap (Paracchino et al., 2011; Su et al., 2017).

Cu_2O nanoparticles can have different shapes, as cubic, octahedral, rhombic dodecahedral, truncated octahedral and 18-facet polyhedral. The basic low-index facets of this materials are (100), (111), and (110), and their facet-independent properties such as conductivity, stability, and photocatalytic activity have been studied. Cu_2O (100) have shown low photocatalytic activity, while (111) and (110) facets are reported to have higher reactivity, as experimental and DFT studies demonstrated. These low-index facets are influenced by the shape, the rhombic dodecahedral show a predominant (111) index facet (Su et al., 2017).

Table 1. Photocathode-Microbial Fuel Cell Systems review

Author	Year	Configuration	The objective of the study	Cathode Material	Anode Material	Maximum power output	Reference
Li, Yan	2009	Dual-chamber	Cr (VI) reduction with simultaneous power generation	Rutile coated cathode for MFC	Unpolished graphite plate	-	(Yan Li et al., 2009)
Lu, Anhuai	2010	Dual-chamber	Semiconductor integration as a cathodic catalyst to enhance the electron transfer	Rutile coated cathode for MFC	Graphite	12.03 W/m^3 Light 7.64 W/m^3 Dark	(Lu et al., 2010)
Chem, Qing-Yun	2013	Dual-chamber	Hydrogen production	TiO_2 nanorod arrays coated upon FTO substrates	Carbon fibre brush	6 mW/m^2	(Chen et al., 2013)
Wang, Siwen	2014	Dual-chamber	Electricity production	fluorine-doped tin oxide (FTO) $CuInS_2$ flower like cathodes	Carbon granules	0.108 mW/cm^2	(S. Wang et al., 2014)
Sun, Zhe	2015	Dual-chamber	Evaluate the effect of photocathode in the electricity generation	CuO nanowires grow in a copper foil	Carbon fibre brush	46.44 mW/m^2 Light 36.99 mW/m^2 Dark	(Sun et al., 2015)
Jiang, Chaojie	2016	Dual-chamber	Destruction of methylene blue and tetracycline	Fe/TiO_2 chemical reduction deposition upon a SS wire mesh using a sol technique	Carbon granules	13.72 mW/m^2	(Jiang et al., 2016)
Nordin, Noradiba	2016	Hybrid system	Fenton reactor to degrade azo dye Reactive Black 5 (RB5)	ZnO/Zn syntheses a Zn sheet and stainless-steel cathode	Iron sheet	15.37 mW/cm^2	(Nordin et al., 2017)
Han, He-Xing	2017	Dual-chamber	Degradation of a Nodek azo dye	Pd nanoparticle-modified p-type Si nanowire photocathode	Carbon paper	0.119 W/m^2	(Han et al., 2017)

Table 1. Photocathode-Microbial Fuel Cell Systems review

Author	Year	Configuration	The objective of the study	Cathode Material	Anode Material	Max. power output	References
Guo, Dan	2017	Dual-chamber	Hybrid system for energy conversion	CuS photocathode	N-doped graphene	1890 ± 8 mW/m^2 Dark 2607 ± 13 mW/m^2 Light	(Guo et al., 2017)
Tuoach, N.	2017	Single chamber	Heavy metal wastewater treatment	Lithium niobite ($LiNdO_3$)	Carbon cloth	131 mW/m^3	(Touach et al., 2017)
Li, Yihua	2017	Dual-chamber	MFe_2O_4 photocatalyst (M=Ni, Fe, Co, Zn) behaviour comparison for wastewater treatment	Carbon nanofiber coated with Composite membrane $CoFe_2O_4$(-rGO) and polyvinylidene fluoride (PVDF)	Granular graphite with a carbon rod	942 mW/m^3 Light 871 mW/m^3 Dark	(Yihua Li et al., 2017b)
Han, He-Xing	2018	Dual-chamber	Hexavalent chromium Cr(VI) reduction for wastewater treatment	Pb-decorated p-type silicon nanowire	Carbon felt	0.175 W/m^2 Light 0.125 W/m^2 Dark	(Han et al., 2018)
Bhowmick	2018	Hybrid system	Evaluate the Bismuth impregnation and its influence on photocatalysis TiO_2 cathodes	TiO_2 (Bi-TiO_2) Bismuth impregned TiO_2	Carbon felt	224 mW/m^2 Light	(Bhowmick et al., 2018)
Wang, Lohong	2018	Dual-chamber	Gas phase VOC ethyl acetate removal and generate electricity simultaneously UV light	TiO_2 nano sheets air cathode deposited upon carbon fiber cloth and PVDF membrane layer	Graphite rod	59.6 mW/cm^2 PVDF 59.6 mW/cm^2 PEM	(L. Wang et al., 2018)
Wu, Jung-Chen	2018	Dual-chamber	Bio-E-Fenton MFCs to evaluate Dairy oily wastewater	Fe_2O_3 dispersed	Carbon felt	52.5 mW/m^2	(Wu et al., 2018)
Ampudia Castresana, Pablo	2019	Single chamber	Electricity generation	CuO-Cu_2O deposited upon FTO and with Nafion layer	Carbon Felt	2.5 mW/m^2	(Castresana et al., 2019)

Table 1. Photocathode-Microbial Fuel Cell Systems review

Author	Year	Configuration	The objective of the study	Cathode Material	Anode Material	Max. power output	References
Jia, Yuhong	2019	Single chamber	Enhance the Cu_2O stability by a carbon coated Cu_2O cathode	Electrodeposited Cu_2O on carbon felt	Carbon Felt	249 mW/m^2 Light 186 mW/m^2 Dark	(Jia et al., 2019)
Guo, Dan	2019	Dual-chamber	Enhance electricity generation in a Light Assisted MFC system	3D Cu_2O @ plasmonic Au nanowire	Carbon Paper	2315.7 mW/m^2	(Guo et al., 2019)
Li, Xiujuan	2019	Single chamber	Photocatalytic evaluation for generating power in a MFC	Nanorod semiconductor metal oxide beta-Ga_2O_3	Carbon felt	1843 ± 40 mW/m^2	(X. Li et al., 2019)

However, the disadvantage of Cu_2O is its photocorrosion, due to the material produces redox reactions, converting the material into a more oxidized or more reduced form of itself. Many efforts have been done to reduce Cu_2O photocorrosion, the most common is adding a thin TiO_2 layer over the Cu_2O materials to act as an electron trap. Another method is to use organic compounds as electron acceptors trying to emulate the photosynthesis electron acceptors to transport the electron to the oxidant present in the catholyte (Freeman et al., 2020).

Ampudia Castresana et. al. used a Nafion layer over a Cu_XO dispersed film to explore the possibility of avoiding corrosion with the Nafion resin to prevent the diffusion of redox interferences to the cathode and as leaching protection for the cathode. Its photoelectrochemical characterization showed a high produced photocurrent under light conditions. The implementation of Cu_XO with Nafion membrane in an SMFC show a lower photocurrent production but better stability in long-term operation (Castresana et al., 2019).

$LaFeO_3$

Perovskite compounds are recently popular due to their potential in several chemical processes such as solar cells, dye degradation and solar water splitting. However, they have been limited due to their instability, especially in the presence of water and their toxicity. For this reason, perovskite oxides for PEC solar water splitting applications have been studied as an alternative material due to their abundance of starting materials and high structural flexibility. Ferrite perovskites are now the most promising materials for PEC processes because they have smaller band gaps and in consequence absorb within the visible light region (Freeman et al., 2020).

$LaFeO_3$ (LFO) has a bandgap between 2.1 and 2.6 eV, it has been utilized as p-type photocathode for oxygen and water reduction under visible light showing a very low photocurrent (Thirumalairajan et al., 2015).

A recent study found that the incorporation of a polymer template improves films quality, increasing the surface area, enhancing the photocatalytic activity. The incorporation of polymer template to growth films consists of a graft copolymer dispersed with metal oxide precursors to act as a template on calcination upon a glass substrate, this metal oxide precursors form nano-size micelle structures. After high-temperature calcination, the polymer is removed, and the result is a highly porous and uniform metal oxide structure (Díez-García & Gómez, 2017; Freeman et al., 2020).

Freeman et al. (Freeman et al., 2020) found that the polymer template prepared LFO films have a faster rate of charge extraction and higher photocurrent efficiency (IPCE), which contribute to the increase of observed photocurrents. Additionally, the polymer template prepared via spin-coating

of metal oxide precursors combined with a non-ionic surfactant Triton X-100 films showed the highest photocurrent density production and showed more photocurrent stability compared to other preparation methods.

LFO photoactive films have not been used as cathode in MFCs systems and they have shown potential properties to increase the stability in the current production of MFC with photoactive cathodes.

Concluding remarks

Microbial Fuel Cells are systems which depend on multiple variables. Nevertheless, research showing the activation losses at the cathode, specifically ORR activation losses is the most significant limiting factor for MFC systems, and many efforts to reduce them have been made. Catalyst and biocatalyst have been implemented before to enhance the MFC behaviour. Recently, photocatalyst addition at the cathode has been implemented as an innovative and promising way to improve the system performance. The photocatalyst at the cathode must be active in the visible region, stable and feasible to implement. For that reason, the implementation of a different photoelectroactive material as a replacement of graphite felt cathode is what this study focuses.

Chapter 2 - Methodology

Synthesis and characterization of semiconductor films

Synthesis of Cu_2O semiconductor films

The cuprous oxide nanoparticles were synthesized by the reaction of $CuSO_4$ with NaOH, and D-glucose in the presence of the organic modifier polyvinylpyrrolidone (PVP Mr 40k). In a Pyrex beaker, 35.0 mL of distilled water were mixed with 2.0 mmol of $CuSO_4 \bullet 5H_2O$ and 20 g of PVP and stirred vigorously until dissolved completely. After that, 8.0 ml of NaOH and 1.0 mmol of D-glucose were added to the previous solution and the mix was stirred until complete dissolution. The final solution was put in an oven at 50 °C for 60 min with the lid tightly closed. Then, the bottle was removed from the oven and let it cool at room temperature. The associated PVP particles were eliminated by washing the final product, firstly with distilled water with 5 min of sonication, and centrifugation at 10,000 rpm by 5 min, all steps of this protocol were repeated 3 times and was finished by rising with 10 ml of ethanol with sonication and centrifugation at the same time. Finally, the obtained nanoparticles were added to a 1 ml of isopropanol and then was sonicated for 10 min.

Figure 6. Cu_2O nanoparticle solvothermal synthesis solution before centrifugation.

Nanoparticles deposition upon the substrate was made by the doctor´s bladed method. The doctor's bladed solution was prepared with 100% wt. of isopropanol, 0.5% wt. of ACAC (acetylacetonate) and 5.5% wt. of PVP. The solution was stirred until each component was dissolved. To mix the doctor´s bladed solution with nanoparticles, 1 mL was added to a vial with the total amount of the previously synthesized nanoparticles and finally, this mixed solution was dispersed by sonication for 30 min.

A few drops of this solution were added to washed FTO substrates and immediately they were bladed to make a uniform film and then were dried by air at room temperature. The bladed films underwent a heat treatment in a 450 °C preheated furnace for 10 or 12 min to evaporate all the added solvents and surfactants such as ACAC, PVP and isopropanol. After the heat treatment, a colour change from brown to dark colour was observed. Finally, the films were ready for electrochemical measurements.

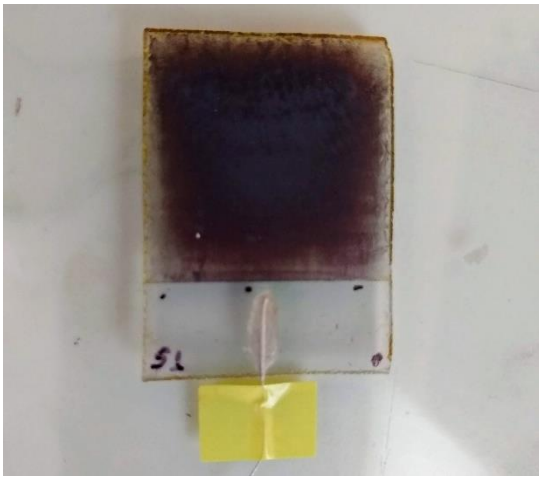

Figure 7. Cu_2O constructed electrode of 9 cm^2 area.

Synthesis of $LaFeO_3$

The synthesis of the $LaFeO_3$ (LFO) was made first with the solution of $LaNO_4$ and $FeNO_4$ and using citric acid as the reducing agent, also, using a mixture of Triton X-100 and tetrahydrofuran (THF) as a polymeric template to make the films via spin coating.

The polymeric template solution was prepared by mixing 1 ml of triton X-100 and 1 ml of THF solutions that were stirred overnight in a closed 5 ml vial. Separately, a solution was prepared by adding 0.2 g of $La(NO_3)_3$ and 0.19 g of $Fe(NO_3)_3$ to 0.5 ml of deionized water, then, the mix was stirred overnight.

Figure 8. $LaFeO_3$ polymeric template solution to prepare the spin-coated films.

Five pre-washed AZO-FTO (Sigma Aldrich®) coated glass pieces were placed in the spin coating machine, a 0.1 ml of the LFO solution was dripped on each glass with a 5 ml plastic syringe and was spin-coated at 4000 rpm for 30 s, then, the solvent was dried by air at room temperature. After that, the films underwent a heat treatment with a 3.8 °C/min temperature ramp until 500 °C for 20 minutes, to remove all the polymer solvents, then the temperature was rising until 600 °C for 3 hours. The spin coating procedure and the whole heat treatment were repeated three times.

Film characterization

The films were structurally characterized by X-Ray Diffraction (XRD) and morphologically characterized by an optical microscope and Scanning Electron Micoscope (SEM).

X-ray diffraction (XRD) patterns were obtained from STOE STADI P double setup, equipped with Mythen detectors, using Cu-Kα1 radiation (lambda = 1.540562 Å) with a range of 2θ from 20 to 80°.

A Keyence Digital Microscope (VHX-7000) was used to obtain information about the surface of the films and a SEM Hitachi SU1510.

Electrochemical characterization

Photoelectrochemical semiconductor film characterization

The electrochemical characterizations were done with a platinum foil as a counter electrode connected to a potentiostat (Ivium CompactStat). A sodium sulphide solution ($NaSO_4$) of 0.5 M (pH = 6.8) was used as a support electrolyte for all measurements. The previously prepared films were used as a working electrode with a 0.25 cm^2 as a working electrode area. A torch lamp of 70 lumens (16 mW/cm^2 of total irradiance at 4 cm distance) was used to illuminate the system. A small cardboard was used to chop the light systematically every 4 seconds.

Figure 9. Quartz cell, electrochemical characterization system.

The Linear Sweep Voltammetry (LSV) test was carried out between 0.0 to -0.6 V at pH 6.8 for the Cu_2O films and 0.2 to -1.1 V at pH 6.8 and at pH 12 to characterize the LFO in dark and light conditions, the system was saturated with oxygen until system equilibrium, in other words, when Open Circuit Potential (OCP) was constant, before each measurement.

Effect on the electrode area

After the general Photoelectrochemical (PEC) characterization, to test the influence of electrode area configuration on the PEC performance, two Cu_2O working electrodes were prepared: 1) a four parallel-connected film configuration and 2) a single big electrode; each of them with the same area (3.8 cm^2). The test was made with Linear Sweep Voltammetry (LSV) between 0.0 V to - 0.6 V, under illumination using a torch LED lamp (16 mW/cm^2) chopping the light with a small piece of cardboard every 4 seconds.

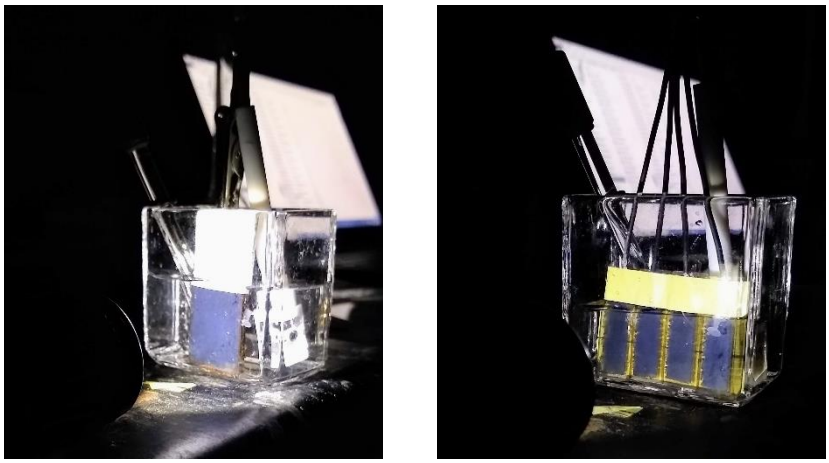

Figure 10. Electrode size performance experiment.

Effect of Nafion membrane resins on PEC characterization

A couple of films were selected to add them to a Nafion resin film to test its influence on them. A 50% wt. solution of Nafion 5% wt. in aqueous resin was prepared and then 0.1 ml of the solution was added to the films; each one was spin-coated at 4000 rpm for 30 seconds, then they were left to dry by air at room temperature overnight before the electrochemical measurements were performed.

The LSV measurements were carried out in the same electrochemical three-electrode cell system ($NaSO_4$ 0.5 M as an electrolyte, Ag/AgCl electrode as a reference electrode and a platinum plate as a counter electrode were used) under illuminated conditions with the torch LED lamp (16 mW/cm^2).

Soil-Microbial Fuel Cell set up

Microbial Fuel Cell Set-Up and test methodology

Anode pre-treatment

First, 18 square graphite felt pieces of 3 x 3 cm were cut. Nine of them were soaked in absolute ethanol 99% for 48 hours, then the pieces were perfectly rinsed and then the graphite pieces were soaked in a prepared solution of ammonium peroxydisulfate 0.87 M and 1.8 M of sulfuric acid for 15 min, then were also perfectly rinsed and stirred 5 min with deionized water 5 times. After that, a heat treatment in a furnace was done at 450 °C for 30 min, with a heat ramp of 10 °C/min. Afterward, the treated electrodes and the remaining electrodes were stitched with titanium wire, making sure that the amount of titanium wire was the same in each electrode.

Building Soil-Microbial Fuel Cells

The soil was collected from University of Bath's Campus surroundings, it was a wooden type soil, then it was hand-cleaned by removing all the branches and leaves. A small amount of soil was put in 600 ml beakers followed of the pre-treated electrode (anode), then, additional amount of soil was put in the beaker covering the electrode and over the added soil the cathode was set in place. The electrode separation was around 4 cm. This procedure was replicated to build the 9 cells. The connections were made in series adding a 500 Ω resistor and then were connected to a measuring system. After setting up the cells, they were monitored each day making sure soil was wet anytime. The SMFC systems were left 4 weeks for the enrichment process that took place at the anode to avoid the instability of anode potential.

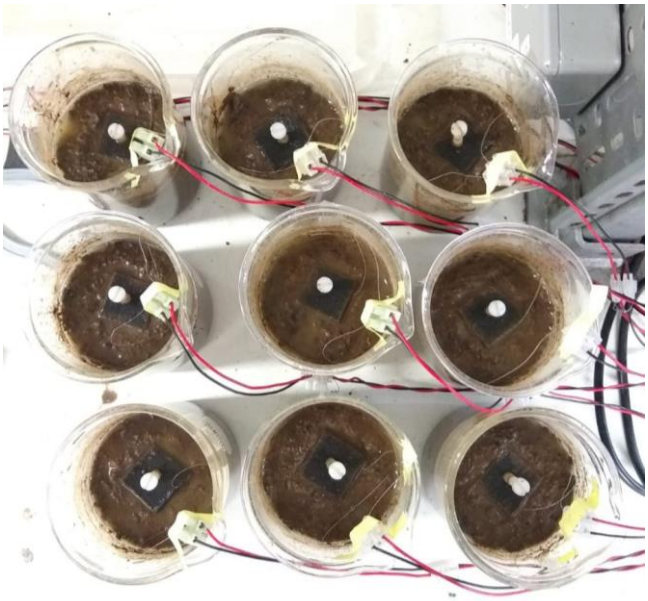

Figure 11. Soil-Microbial Fuel Cells-MFC systems set up.

Design and building light – set up

The light set up was built in a 6 mm MDF tables, in a three-light compartment. A GX53 Lamp (Bonlux) was used, the light intensity was measured at 4 cm distance from the lamp showing a 12 mW/cm^2 value. Each compartment could contain an MFC and was divided to guarantee the same light on each Soil-Microbial Fuel Cell (S-MFC).

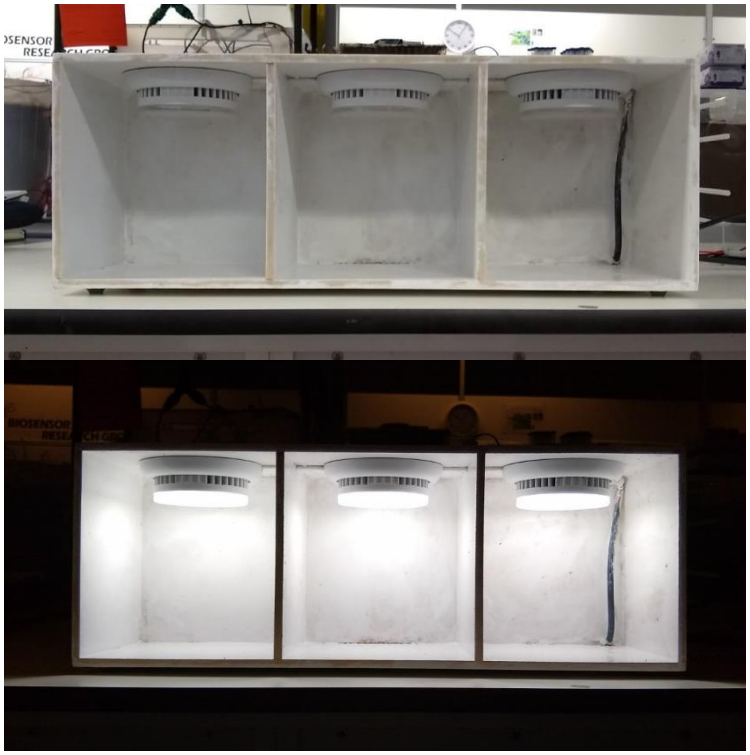

Figure 12. Light cabin set up.

Discharge test protocol for S-MFC

After a four weeks period of enrichment, each SMFC system's polarization test was carried out in groups of three, one group for each cathode replacement that was done. The first step was the connection of the fuel cells system to resistance boxes and set it to 10 MΩ, this value was considered as Open Circuit Voltage (OCP), and the systems were left for 1 hour until the overall cell voltage was stable. Afterward, the discharge test was started decreasing the resistor value and left 5 or 10 min or until the systems showed stability between each cell measurement. At the same time, the individual electrode potential was measured with an Ag/AgCl reference electrode which was set in each system, then the potential between the reference electrode and the anode was registered and the same procedure was applied to the cathode. Both steps were made for each resistor decreasing the resistor value on each measurement. Finally, when we achieved the smallest resistor value, we changed the resistor value to the initial one, in this case, 500 Ω, and we left it to stabilize 16 hours approximately to continue with the cathode replacement and light and dark polarization test.

Cathode replacement and dark and light discharge test

The cathode replacement was carried out the next day after the polarization test. Firstly, the graphite felt cathodes were removed from 3 of the SMFC systems and the photoactive cathodes were set in place over the soil with the conductive part of FTO facing the soil, an additional reference

electrode embedded in the soil was put near the electrodes. When the three SMFC systems were connected to the measurement system and the resistor boxes, the beakers were setting in place at the light set up, and immediately the light was turned on, the value of the resistor was set to the open circuit value and after 60 min the test followed the same protocol as the graphite felt discharge test but the resistor value window between 200 kΩ – 5 kΩ for the Cu_2O cathode system, 200 kΩ – 1 kΩ for Cu_2O with Nafion layer system, and 200 kΩ – 5 kΩ for LFO system. Finally, when the discharge test was finished the light was turned off and the systems were set at open circuit resistor value and the discharge test was made again after 60 min of stabilization but now in dark conditions.

Figure 13. System after cathode replacement and implemented in the light set-up.

Light and dark cycle output potential characterization

Afterward the discharge tests, the external resistor value was set to 40 kΩ and dark and light 6 hours cycles were programmed with a timer. In total, 3 dark-light cycles (6 hours under light conditions and 6 hours in dark conditions) were carried out. The overall potential of each photocathode system was registered to see how it changed in dark and light conditions.

Figure 14. The system in the light set-up.

Chapter 3 - Results and discussion

The objective of this thesis project was to explore the use of photoelectroactive materials implemented in a Soil Microbial Fuel Cell. Both visible-region photoactive materials were selected: Cuprous Oxide (Cu_2O), and Lanthanum Ferroxide $LaFeO_3$. These materials were selected to use visible solar light to drive the Oxygen Reduction Reaciton (ORR) at the cathode, which is the limiting factor in SMFC, and in consequence enhance SMFC performance.

Depending of the nature of the semiconductor (if it is n-type or p-type), when it is radiated by light and if the energy of photons is higher than the band gap of the material the photon will be absorbed by the material and an electron from the valence band will be exited to the conduction band. In other words, electrons in valence are excited into the conduction band leaving holes in the valence band, electrons and holes are photo-generated and are semiconductor's charge carriers. Depending of the nature of the semiconductor, minority and majority carriers will be generated. This phenomenon is the basis of photovoltaic production of energy, and light-assisted semiconductor applications. The photo-generated electrons cause reduction reactions and photo generated holes cause oxidation reactions. This process is described in the diagram of Figure 15. In the case of Cu_2O and $LaFeO_3$ as a p-type semiconductor which have excess of holes in their structure, will be used as photocathodes for reduction reaction, specifically to enhance the ORR at the cathode. To achieve this enhanced reaction, the conduction band must be located at a more negative potential than the reduction potential of ORR which is reported as 1.23 V via $4e^-$ to produce H_2O directly, and 0.63 V via $2e^-$ to produce H_2O_2. However, here is an activation barrier in the charge-transfer process between photocatalyst and water molecules of electrolyte, for that reason photon energy must be greater than band gap energy necessarily to drive the ORR.

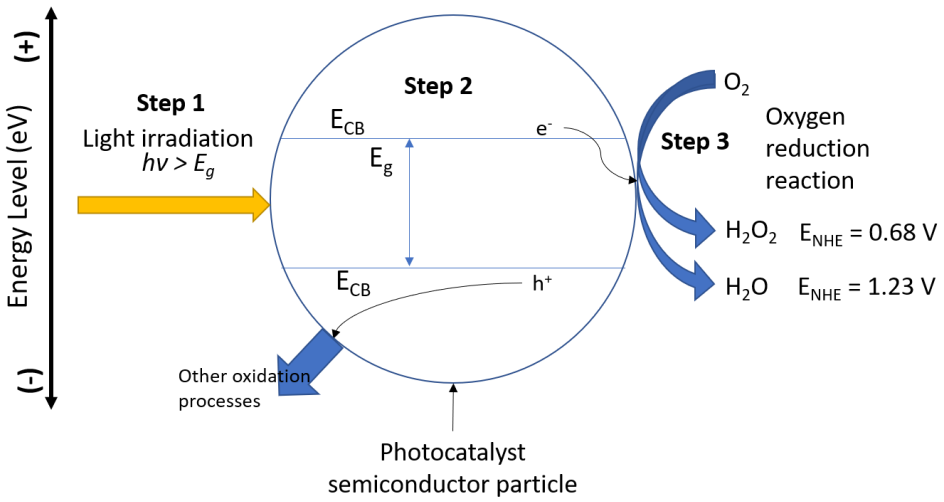

Figure 15. Photocatalysis process diagram. The first step is the irradiation with an energy which is higher than the band gap of the semiconductor, the second step is the charge charrier separation, the absorbed photon energy generates charge carrier's separation generating electrons and holes which cause different electrochemical processes. In the Step 3, photo-generated electrons cause different ORR reactions depending on the electrochemical potential. In this case it is necessary 1.23 V electron energy to reduce the oxygen via 4e⁻ and 0.68 V to reduce oxygen via 2e⁻.

The selected materials for this study have in common that they absorb light in the range of visible light spectra. Cu_2O is p-type semiconductor material which it bandgap energy is between 1.2 to 2.1 eV (Ampudia et al., 2019) and it depends of the crystal characteristics like morphology and crystallinity. $LaFeO_3$ is a metal oxide with a perovskite structure and its bandgap is around 2.5 eV. These band gap magnitudes are equivalent in magnitude in the visible light spectra, see Figure 16.

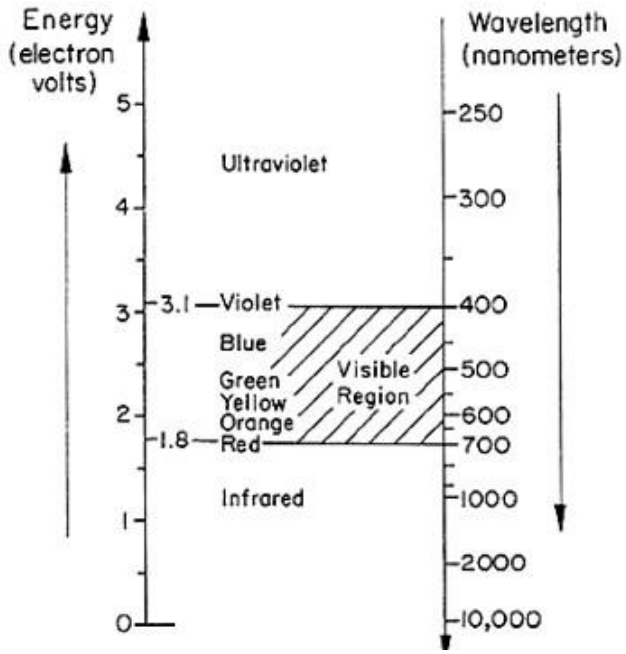

Figure 16. Electron energy to wavelength conversion diagram (Muller, 2007).

The use of three different arrays of photocatalyst was investigated to improve electrochemical performance of Soil-Microbial Fuel Cells. Three different types of cathodes where tested in three different soil microbial fuel cells. GF, FTO/Cu_xO, FTO/Cu_xO/NF and we introduced a new cathode material which was $LaFeO_3$ (LFO), FTO/LFO. In the next paragraphs, results and discussion firstly of structural and morphological characterization, photo-electrochemical characterization and results where the photoelectrode was implemented in SMFC are presented.

Morphological and structural characterization: High-resolution optical microscope and X-Ray Diffraction (XRD)

The morphology of the Cu_xO-based photocathodes is shown in Figure 17 and Figure 18A, where the morphology is characterized by tetrahedral-shape granular film, with particle size below 3 µm. The SEM images confirmed the Cu_xO tetrahedral-shape nanoparticles film that is easily observed in Figure 18A. When the Nafion layer was added to the nanoparticle film (Figure 18B) the uniformity increases on the dispersion of nanoparticles and in consequence on the electroactive surface; moreover, in Figure 18C $LaFeO_3$ film showed a great uniformity additionally. In the Figure 18D a nanopore dispersion on the $LaFeO_3$ film could be observed, the presence of nanopores in the $LaFeO_3$ has been observed as a property of perovskites films (Freeman et al., 2020).

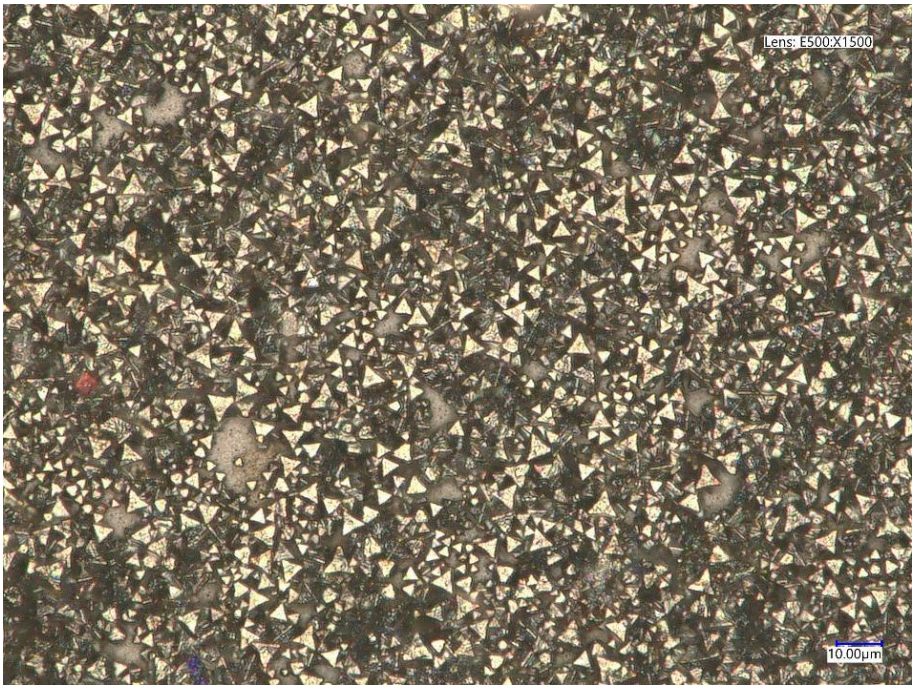

Figure 17. Cu_2O film surface photo obtained with a high-resolution optical microscope. The tetrahedral shape of the nanoparticles is observed.

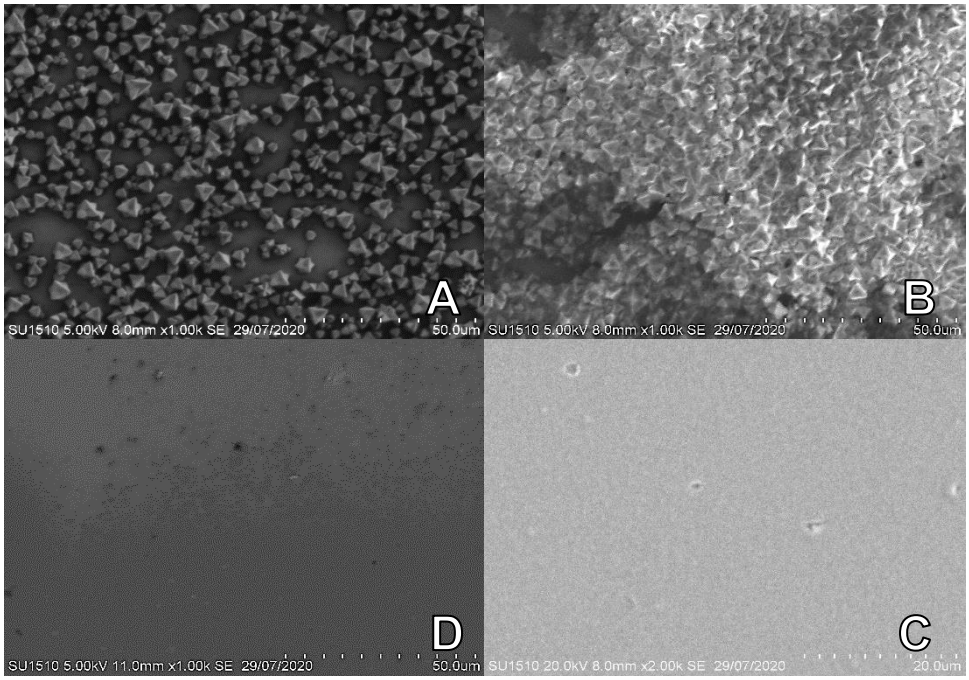

Figure 18. SEM images of semiconductor thin films: A) Cu_2O, B) Cu_2O + Nafion, C) $LaFeO_3$, D) $LaFeO_3$ zoom.

The XRD pattern of the cooper oxide film deposited by doctor-blade method Fluored-doped Tin Oxide (FTO) glass, after thermal treatment at 500 °C is displayed in Figure 19. The film pattern of the FTO/Cu_xO electrode clearly shows peaks at 2theta = 29.6, 2theta = 36.5, 2theta = 42.34, 2theta = 51.49 which correspond to (110) Cu_2O, (111) Cu_2O, (200) Cu_2O, (112) CuO crystal planes, respectively. The (111) following with (222) plane are the one with highest area due tetrahedral shape of nanoparticles (M. A. Khan, 2015).

In previous simulation studies (Su et al., 2017), the theoretical optimum simulation planes of photocatalytic conversion of Cu_2O were determined concluding that the predominance of (111) and (110) plane in the crystal structure will give to the material an optimal photocatalytic behaviour because these crystal planes expose more atom quantity to the surface of the material, it enhances the interactions with electric fields of each atoms, enhancing light interaction and electron transfer. Figure 19, shows perfectly that the predominant plane is (111) and its linear combinations form the tetrahedral shapes of Cu_2O nanoparticles showing in Figure 18A.

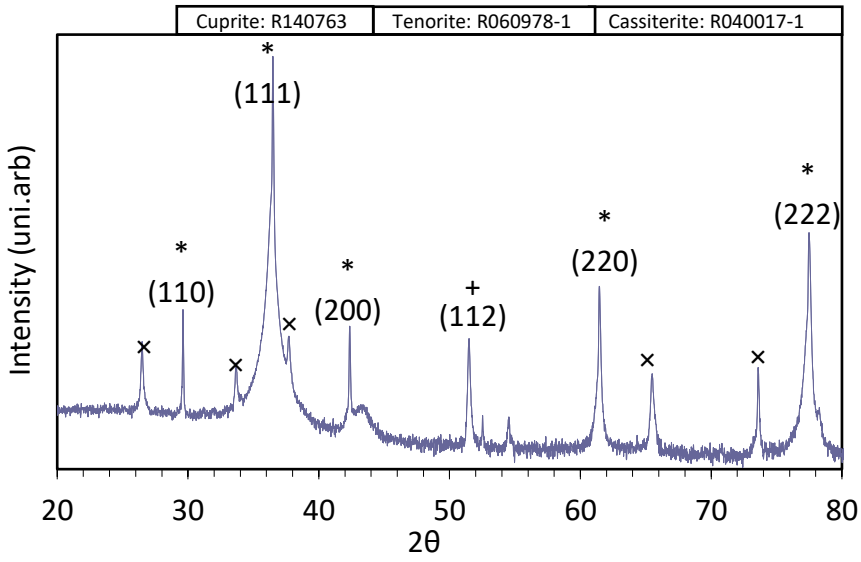

Figure 19. X-ray diffractograms of Cu_2O, prepared by the bladed solvothermal synthesized nanoparticles. The "" represents the Cu_2O crystal structures, "+" represents the results of the CuO, and the "x" represents the FTO structure.*

The film pattern of FTO/$LaFeO_3$ electrode is shown in Figure 20, where it clearly shows peaks at 2θ = 34.05, 2θ = 38.37, 2θ = 51.72, 2θ = 61.94 which correspond to (021), (103), (114), (231) $LaFeO_3$ crystal planes, respectively. The perovskite planes are not uniform because the cubic-perovskite base is not totally cubic, these is due a crystal deformation in the annealing process (Cullity, 1978).

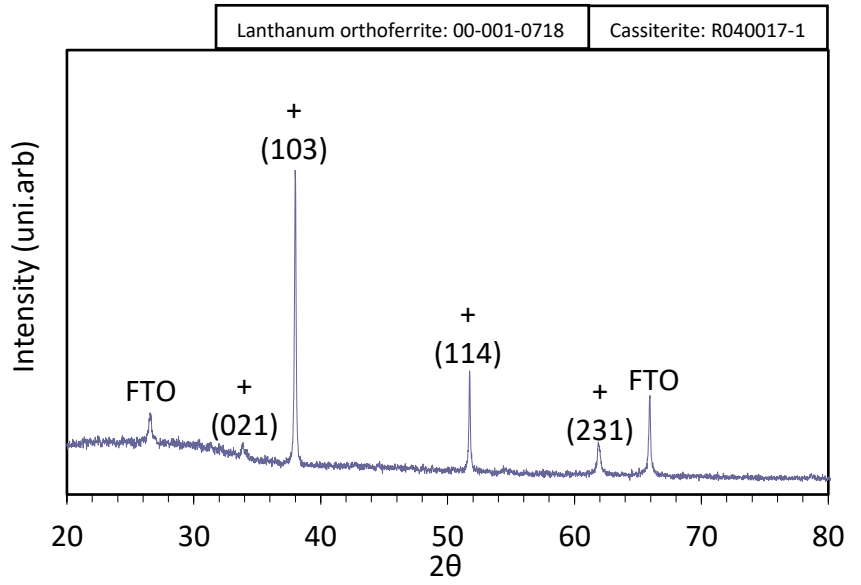

Figure 20. X-ray diffractogram of $LaFeO_3$ thin films synthetized via spin-coating with a polymer template. The "+" represents the perovskite film structures.

Electrochemical characterization

Photoelectrochemical characterization

The three prepared electrodes were electrochemically characterized by LSV, under irradiation in an aqueous solution containing 0.5 M of Na_2SO_4 (pH = 6.8). In the Figure 21 and in Figure 22 an increase in the reduction current under radiation conditions can be observed, this phenomenon confirms the photoactivity of Cu_xO and $LaFeO_3$. But the order of the photo-current generation is higher in Cu_xO because the highest difference between dark and light conditions in current is around 1.96 mA/cm^2 and for LFO is in 0.06 mA/cm^2 approximately. In the case of Cu_xO, the photogenerated current was comparable to the Cu_xO previously used for the similar application, where the photocurrent difference was around 2.00 mA/cm^2 (Ampudia et al., 2019). Additionally, the photocurrent production is similar to other Cu_2O results reported in the literature (Schreier et al., 2015). Moreover, $LaFeO_3$ photocurrent production is comparable to the result reported in the literature (Freeman et al., 2020), additionally, the earlier starting on photocurrent generation (Figure 22) in the $LaFeO_3$ at lower applied potentials which was observed in other works was also present in this work.

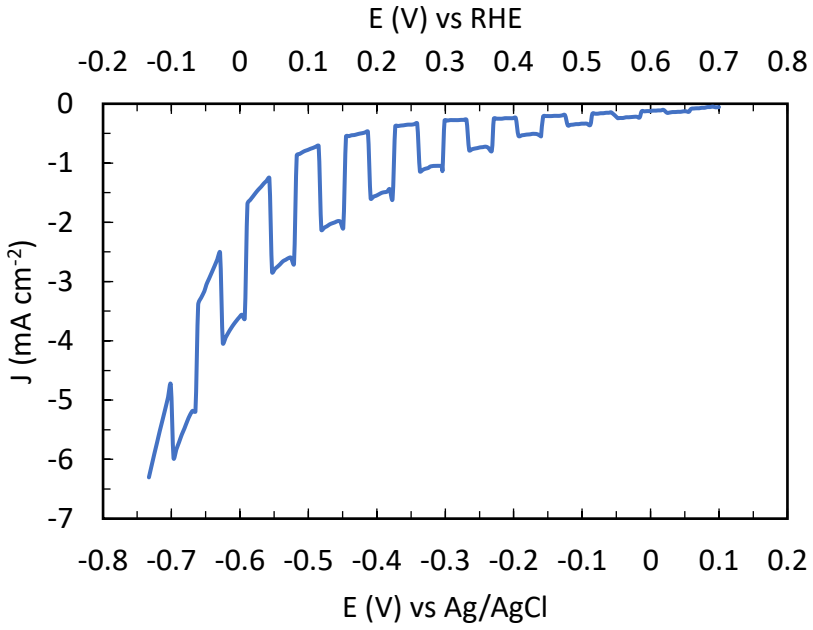

Figure 21. Cu_2O films PEC LSV characterization using a Na_2SO_4 0.5 M, and Ag/AgCl as a reference electrode and a platinum plaque as a counter electrode, using a 300 W Xe lamp equipped with an AM1.5G solar simulator filter to illuminate the system.

The shape of the curves shows that electron transfer for species reduction starts earlier in both materials. In case of $LaFeO_3$ LSV curve the photocurrent starts in more positive applied potentials, since 0.2 V vs Ag/AgCl (0.8 V vs NHE) or earlier. In case of Cu_xO the electrons transfer starts approximately at 0.0 V vs. Ag/AgCl equivalent to 0.6 V vs. NHE, this potential is the ORR potential via

$2e^-$ to H_2O_2. This curve means that the oxygen reduction reaction needs less energy under light conditions than dark conditions because the electron transfer is enhanced.

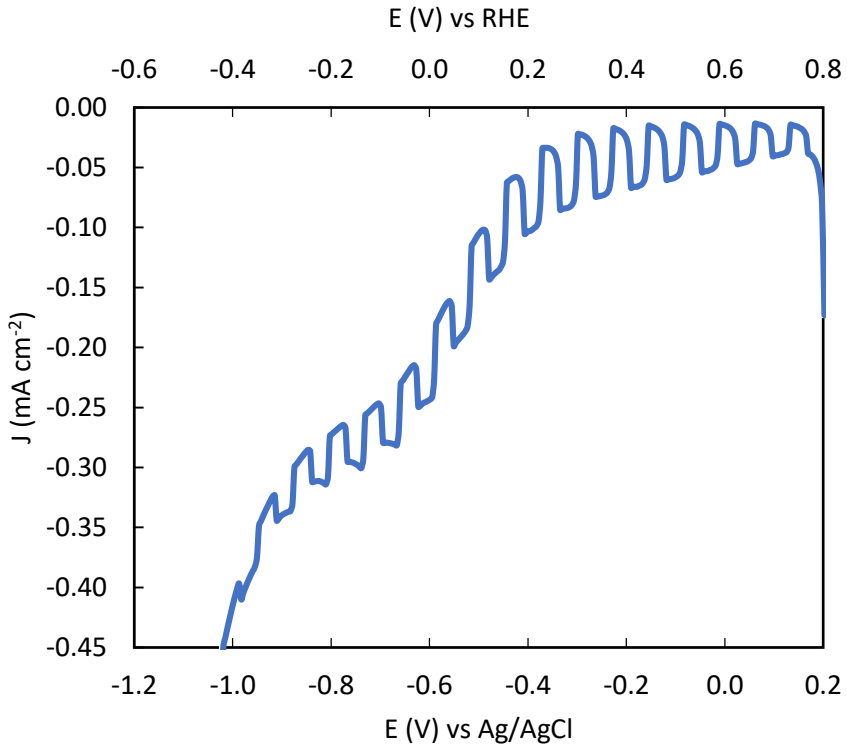

Figure 22. $LaFeO_3$ films PEC LSV characterization using a Na_2SO_4 0.5 M, and Ag/AgCl as a reference electrode and a platinum plaque as a counter electrode and using a 300 W Xe lamp equipped with an AM1.5G solar simulator filter to illuminate the system.

Generally, SMFC works at pH > 7 because soil has a pH between 5 and 7 (Dziegielowski, 2018). Previously studies reported that $LaFeO_3$ is more photo-active and stable in alkaline electrolyte conditions (Freeman et al., 2020), this experiment reports the difference between photoelectroactivity at both pH conditions, alkaline and neutral pH to demonstrate the $LaFeO_3$ could be applied for SMFC devices. On the other hand, these measurements were also carried out under Nitrogen and Oxygen saturated conditions to test the ORR activity.

The results of the linear voltamperometry study of the present work are shown in Figure 23. The experiment was carried out with the objective to evaluating the oxygen reduction potential on LFO films electrodes. It is important to mention that a torch LED lamp of 6 mW/cm^2 was used for these studies. For this reason the curves show remarkably lower photoelectroactivity on the difference of photocurrent production under light and dark conditions. The LFO samples saturated with N_2 gas showed less electroactivity than the system saturated with O_2 due of the absence of electron acceptor in the electrolyte (O_2). The LFO electrochemical systems at pH 12 conditions demonstrate more

stability in photocurrent generation along the measurement under dark and light conditions, instead of the pH 6.8 conditions which exhibit low stability in photocurrent generation under both conditions. Additionally, both pH condition curves which are saturated with O_2 display an ORR peak. The most pronounced and stable curves are at pH 12 condition which show a reduction peak at 0.77 V vs. Ag/AgCl reference electrode (0.16 V vs NHE), in contrast with pH 6.8 that show earlier electron transfer activity in lower positive applied potentials, at 0.7 V vs Ag/AgCl (0.06 V vs NHE). $LaFeO_3$ is unstable in lower pH because acidic medium causes film corrosion, and it was demonstrated that in alkaline solution, the photoactivity electron transfer is optimum (Freeman et al., 2020). However, $LaFeO_3$ cathode photo electrochemistry performance at pH = 6.8 is enough for soil microbial fuel cells electrode application.

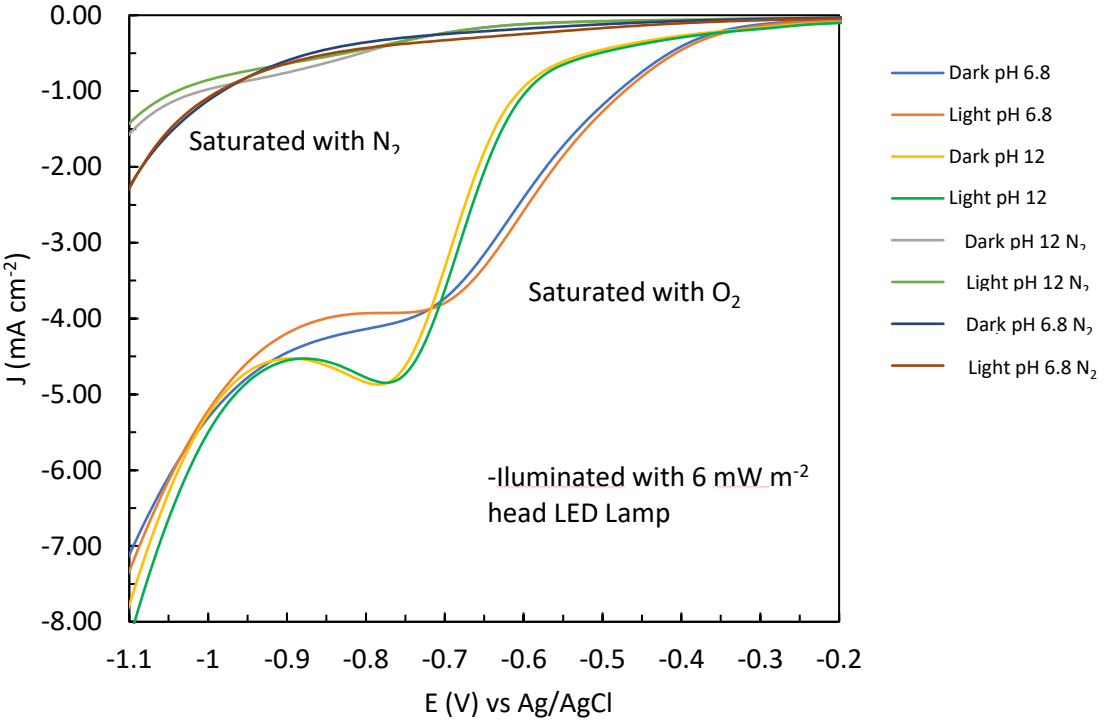

Figure 23. $LaFe_2O_3$ performance at pH 6.8 and pH 12 with a system saturation of N_2 and O_2. A Na_2SO_4 0.5 M was used as an electrolyte, an Ag/AgCl electrode as a reference electrode, and a platinum plaque as a counter electrode. The system was illuminated with a 6 mW cm^{-2} small LED lamp.

The final experiment setup, where the photocathodes were implemented in a SMFC systems and tested under dark and light conditions, uses LED lamps with 10 mW/m^2 of intensity each. Consequently, it was necessary to prove that the used materials have photoactivity under lower light intensity and pseudo-neutral pH conditions.

Figure 24 shows the comparison between the LSV Curve of Cu_2O film and LFO film in dark and light conditions at same pH = 6.8. The generated photocurrent is higher in the system with Cu_2O, which

shows a photocurrent density difference of 1.87 mA cm^{-2} while $LaFeO_3$ showed a 0.15 mA cm^{-2}. These results are coherent with the previously obtained results using the Xenon Lamp (Figure 21 and Figure 22). This result proves that both materials have comparable photoactivity under lower light intensity and same pseudo-neutral pH. Due to this behaviour, they could be applied as a photo-cathode compatible for biological applications and in consequence for Soil Microbial Fuel Cells systems.

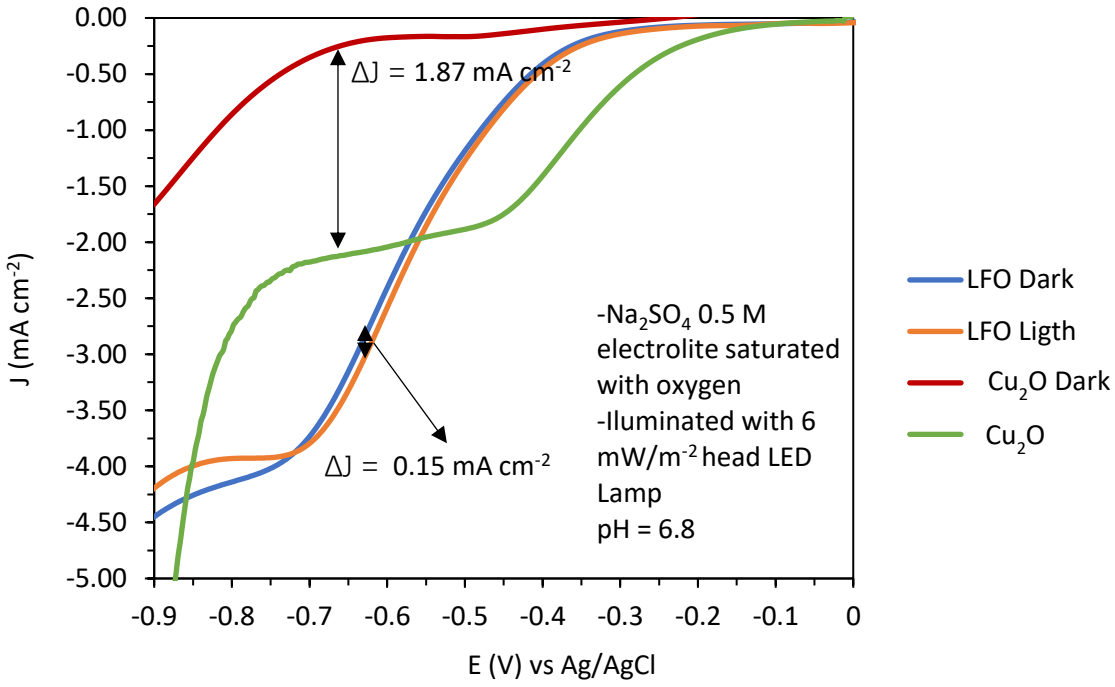

Figure 24. Cu_2O and $LaFeO_3$ LSV curves comparison with saturated O_2. A Na_2SO_4 0.5 M was used as an electrolyte, an Ag/AgCl electrode as a reference electrode, and a platinum plaque as a counter electrode. The system was illuminated with a 6 mW cm^{-2} small LED lamp.

Effect on the electrode area

Electrode area is another important parameter to standardize in SMFC test because some studies in inorganic photo-electrocatalysis fuel cells have shown that if the photo-electrocatalyst area increase, decrease the photoelectrode performance (Hankin et al., 2017). However, the electrode area arrays for Soil Microbial Fuel Cells are explored for the first time. As it was described in the methodology, two arrays with the same area were constructed: a single big electrode, and an array of 4 electrodes connected in parallel. This experiment was made with the objective to select which array shows the best performance to design the final electrodes for Soil-Microbial Fuel Cells devices.

This experiment shows that a single 3 x 3 cm electrode display more photoelectroactivity than the small electrodes array, as is shown in Figure 25. This can be due to the several ohmic resistances

which are created between wires and electrode surfaces in the small electrodes array which prevent an efficient electrode transport.

The single electrode can have more uniform electron transport and reacts more efficiently under light conditions. Previous modelling and experimental studies about the effect of area on photocatalysis concluded that on areas > 0.1m^2 the photoactivity performance drops exponentially, however the photoactivity is not affected in smaller electrodes (Hankin et al., 2017).

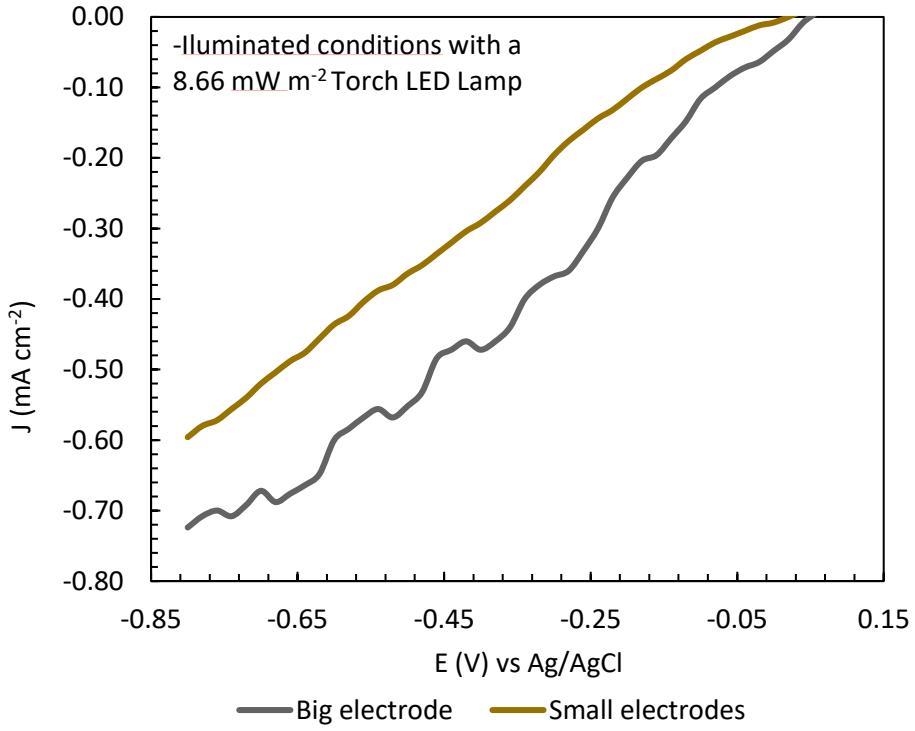

Figure 25. Cooper Oxide Cu_2O Electrode area configuration comparison. A Na_2SO_4 0.5 M was used as an electrolyte, an Ag/AgCl electrode as a reference electrode, and a platinum plaque as a counter electrode. The system was illuminated with a 16 mW cm^{-2} small torch LED lamp.

Effect with Nafion membrane

Nafion membrane has a big impact on current production as shown in Figure 26. The current production increases considerably in the Nafion added Cu_XO sample due the ion transport properties of Nafion resin. Nafion is a ionomer and it was widely used as a proton exchange membrane in microbial fuel cells due its stability. On the other hand, some elements that compound the polymer chain of Nafion resin have some electronegative molecules as sulfonate acid groups (-SO_3H) and fluorine (F) as part of its chemical composition (Mauritz & Moore, 2004). Nafion properties allow to enhance the electron transfer; additionally, it acts as an electrode protective layer which prevent the Cu_xO leaching to the soil. By enhancing proton diffusion to the photoelectrode surface, the reaction between the electron acceptor species is also enhanced because protons (H^+) and electrons (e^-) from

anode on the photoelectrode/electrolyte interface, in consequence accelerates the consumption of photo-generated carriers and prevents the e^-/h^+ recombination within the Cu_xO layer (Ampudia et al., 2019).

The majority of electrocatalyst studies use Nafion as an adherent in the electrocatalyst paste preparation, combined with carbon nano-powder and a determined amount of a inorganic synthesized electrocatalyst (Borja-Arco et al., 2011). Figure 26 curves show the three distinct regions caused by ORR catalysis on a catalyst surface, this regions are: 1) kinetic region where the current is only dependent of the kinetic processes 2) mixed control region, where the behaviour is determined by kinetic as well as diffusion processes; and 3) mass-transfer region, where the diffusion occurs. In these cases the characterization method did not use a rotating disk electrode, for that reason the diffusion process is not a function of rotation velocity (Borja-Arco et al., 2011). As it is shown in the Figure 26, the ORR starts in 0.6 V vs NHE, but under light conditions the photocurrent increases, this can be due because the mass transport is efficient with Nafion, because the ion pass through the membrane more efficiently.

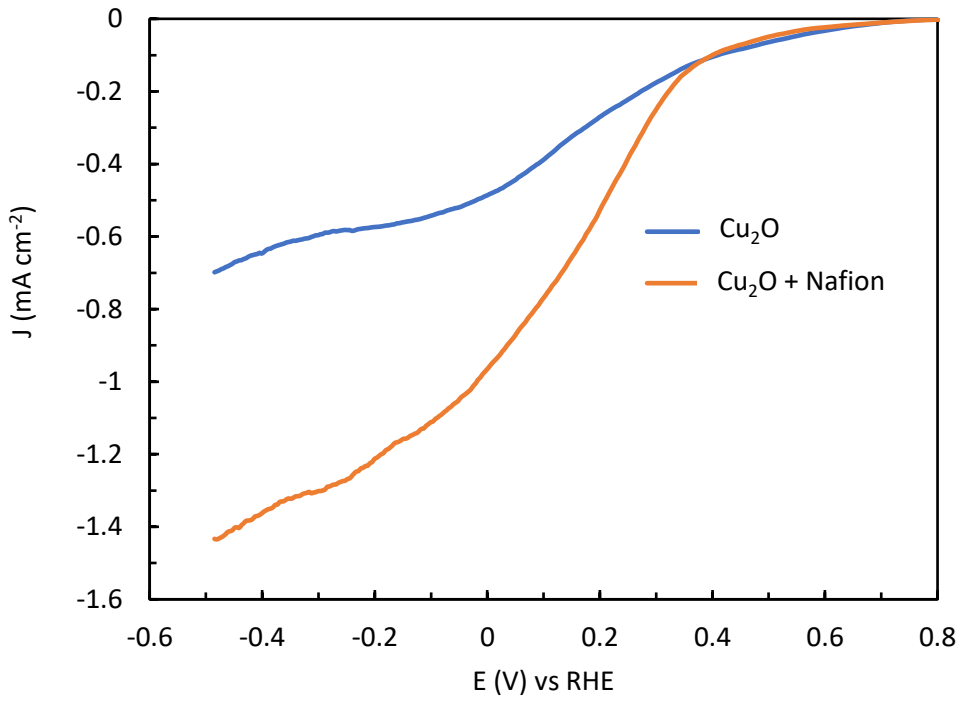

Figure 26. The comparison between without Nafion and with Nafion-added Cu_2O film electrode. A 0.5 M Na_2SO_4 was used as an electrolyte, an Ag/AgCl electrode as a reference electrode and a platinum foil as a counter electrode. The system was illuminated with a 6 mW cm^{-2} small torch LED lamp.

Soil-Microbial Fuel Cells systems characterization

After material characterization, the study proceeds to characterize the SMFC first with graphite felt and then replacing cathode for one of the three different constructed arrays of photocathode: FTO/Cu_xO, FTO/Cu_xO/Nafion and FTO/$LaFeO_3$.

Enrichment period

The SMFC systems were set up, both overall cell and individual electrode potential were monitored with a multimeter each day at the same time with the objective to illustrate how the anode biofilm is created. The cells were operated in a continuous mode where the most important parameters to evaluate are cell stability and when the system reaches the steady state (Dziegielowski, 2018).

After approximately three weeks of operation, a pseudo-stable state on the overall voltage was observed (Figure 27). These data were used to evaluate anode enrichment which refer to electroactive bacteria biofilm formation on electrode surface (Dziegielowski, 2018). The graph shows how electrode potential between cathode and anode increases because anode potential becomes more negative, due the biofilm formation and electron transfer from bacteria membrane to anode. On the other hand, cathode potential becomes more positive due the reduction reactions performed on electrode interfaces, if the catalytic activity of this electrode is efficient, cathode becomes more positive. There are three different phases on enrichment graphs that were also identified in Figure 27. The first one is lag phase which occurs immediately after systems start up and persist until microbes adapted to the new environment. The second phase is called “exponential” phase where the bacteria growths on the electrode, this is where the biofilm is formed. Finally, after the enrichment period, an stable period is expected where the increase is approximately zero and the systems generate stable power (Dziegielowski, 2018).

These results suggest that biofilm was active on anode electrode surface, and the cells were in optimum conditions to apply the discharge test.

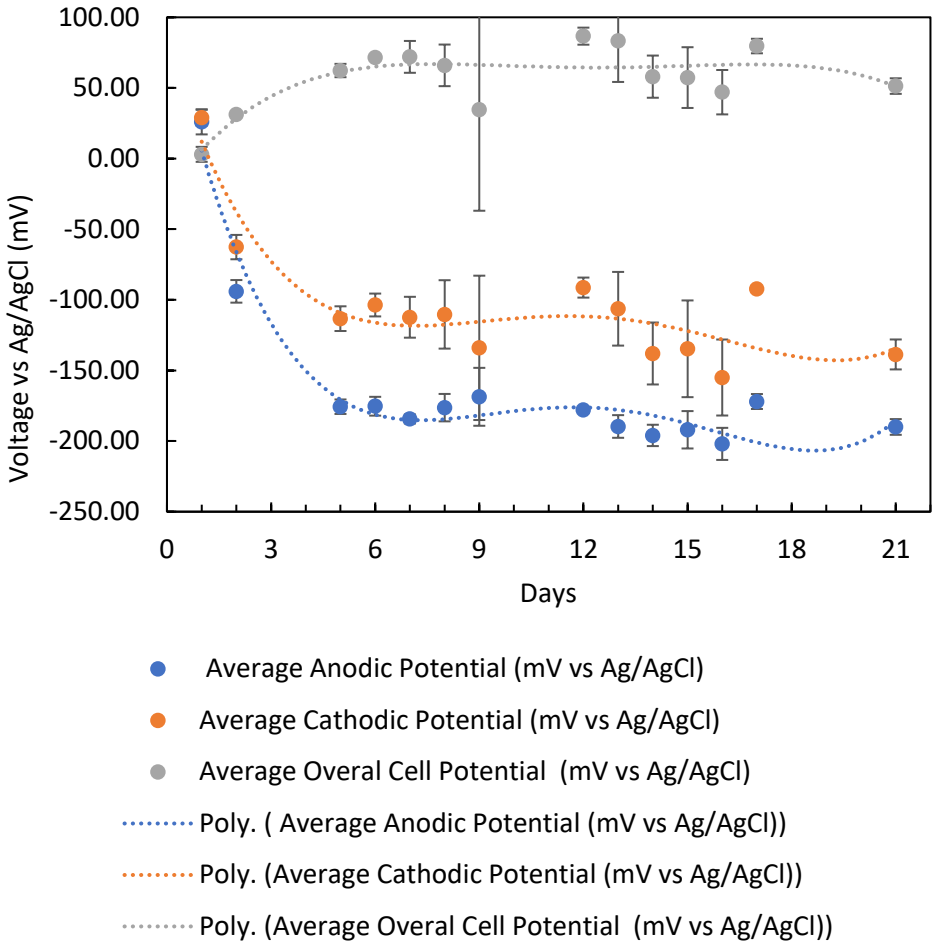

Figure 27. Overall cell potential and individual electrode potential along enrichment period.

Polarization test characterization and calculations

Following enrichment period, electrochemical analysis was made. The polarization test was made using the individual cycle test (with variable resistance). These results were obtained connecting the SMFC systems to a variable resistance controlled by resistor boxes. Later, the overall cell output potential was measured until reaching the pseudo-stable state. The Ohm's law, (Equation (6)), was used to calculate the current corresponding at each voltage value and the power was calculated using the power's law, Equation (7) (Dziegielowski, 2018; Logan, 2008).

$$I = \frac{V}{R} \tag{6}$$

$$P = V \times I \tag{7}$$

The data obtained were utilized to obtain the power curves and the polarization curves. These are powerful tools to characterize MFC systems. They were used to provide information about the

electrochemical profile of the system. The power curves are graphs where power (mW) is plotted against the current (mA), giving information about maximum power output which the system can obtain and its components: maximum current production and its respective voltage. Additionally, other important graph is polarization curve, the analogue of the fuel cells systems. These curves identify the internal resistance with the equation y = mx + c, where y is analogue to electromotive force of the MFC system and the slope, m, is the internal resistance of the system. Polarization curve can be used to interpret the three different types of electrochemical losses exposed in the Chapter 1: activation losses and concentration losses. Analysis of these curves could lead to obtain information about limiting factors of MFC which is crucial for system enhancement (Dziegielowski, 2018; B. Logan, 2008).

$$R_{INT} = \frac{-\Delta E}{\Delta I} \quad (8)$$

Polarization test results

Polarization test were performed after three weeks of anode enrichment period. For testing, the SMFC systems with graphite felt cathode were now irradiated with a LED lamp in a three-compartment light-set-up. It is important to mention that for graphite felt characterization, cathode replacement and dark and light conditions test and dark/light cycles tests where made one at time. First, polarization test with graphite felt cathode was done. The second step was cathode replacement, one cathode material at time were replaced and tested. Then polarization test first under light conditions and when the system was stabilized, the dark conditions measurements were carried out. After the three polarization tests, a 40 kΩ resistor was connected to each system to proceed to the long-term operation dark/light cycle test. Afterwards, each measurement was proceeded to change the light systems. This protocol was followed because the objective was to evaluate the systems behaviour and compare properly photo-cathode performance under light and dark conditions procuring the stability of each system when the cathodes were replaced, the MFC systems tend to be very fragile and variable if the parameters are not well controlled. The systems were tested in the next order: Cu_2O, Cu_2O + Nafion, and $LaFeO_3$. The results obtained from polarization test are described one by one below.

Figure 28 displays the polarization curves of Cu_2O photocathode system, the V_{OC} (Open Circuit Voltage, it means the produced voltage when the current is zero) of illuminated system is 50 mV approximately higher than the non-illuminated system. Moreover, the short circuit current density (I_{SC}, it means the current when the Voltage = 0) is 0.1 μA/cm^2 higher on illuminated conditions than

dark conditions. The difference of V_{OC} and I_{SC} values shows that light helped to reduce activation losses in the system.

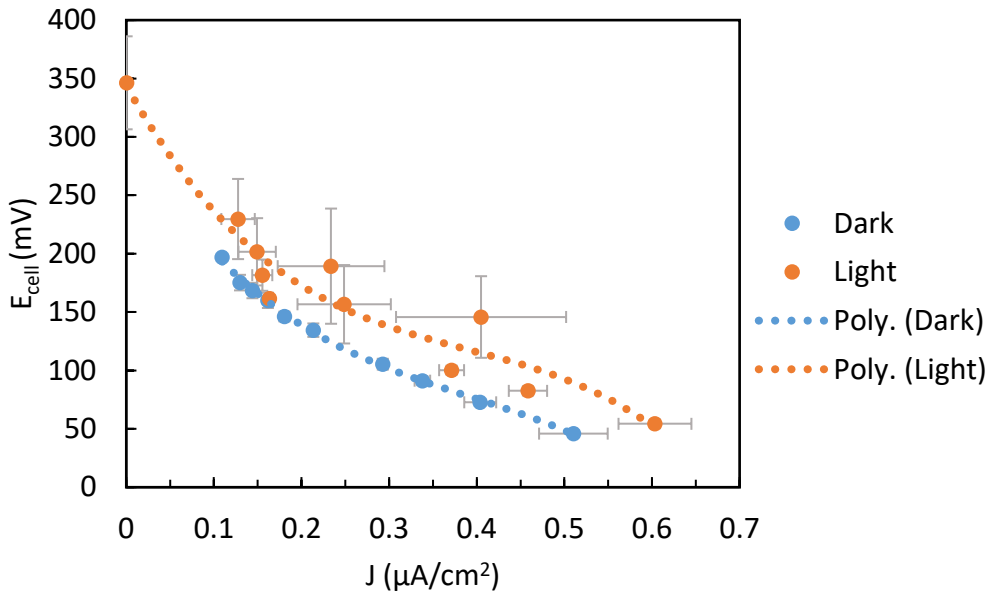

Figure 28. Cu_2O photocathode Polarization Curves comparison in dark and light conditions.

Figure 29 also integrates the graphite felt polarization curve, and displays that cathode have a lower V_{OC} (200 mV less than photocathode system) and a considerable higher I_{SC} compared to photocathode systems, with a difference of 3.5 µA/cm^2 more than photocathode systems. Additionally, a clear dropping in photocathode curves in contrast with GF system is displayed. The curve shapes are attributed firstly to the high catalytic activity on the cathode which decreases activation losses and increases the potential difference between cathode and anode, that is the reason of high V_{OC}. Secondly, the higher internal resistances in the system are responsible to the fast dropping in the photocathode polarization curves, the GF system seems to have less ohmic losses.

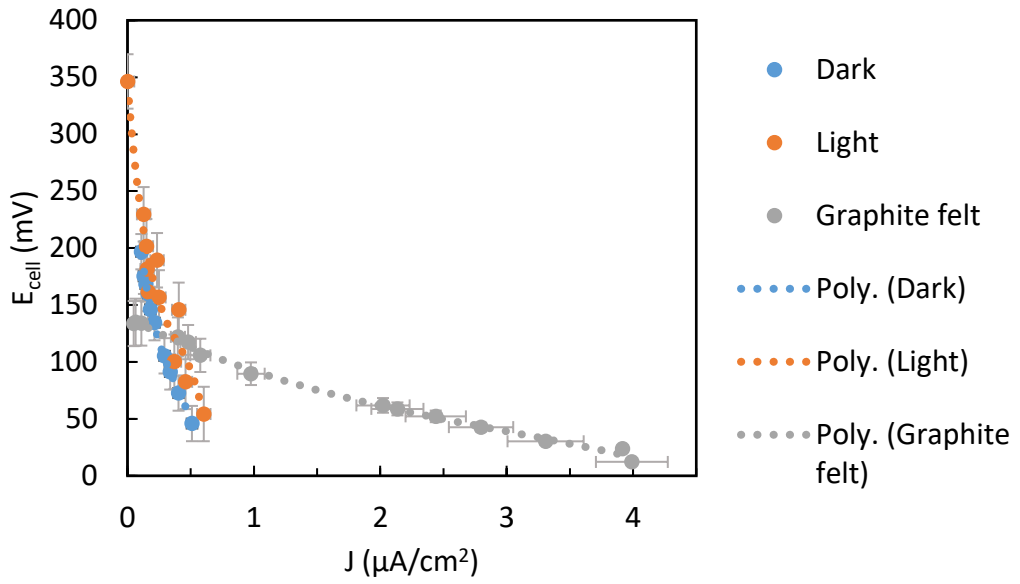

Figure 29. Cu_2O cathode polarization curves vs Graphite Felt cathode.

The comparison of photocathodes system power density curves is displayed in Figure 30 where a difference of approximately 0.02 µA/cm^2 between light and dark conditions is observed. The systems had an unstable behaviour during the light-phase discharge test in contrast to dark-phase which show notably stability during the measurement. This difference could be attributed to the charge carriers that were generated during light conditions are not uniform, but the trend line shows a general better power production performance during light conditions than dark conditions.

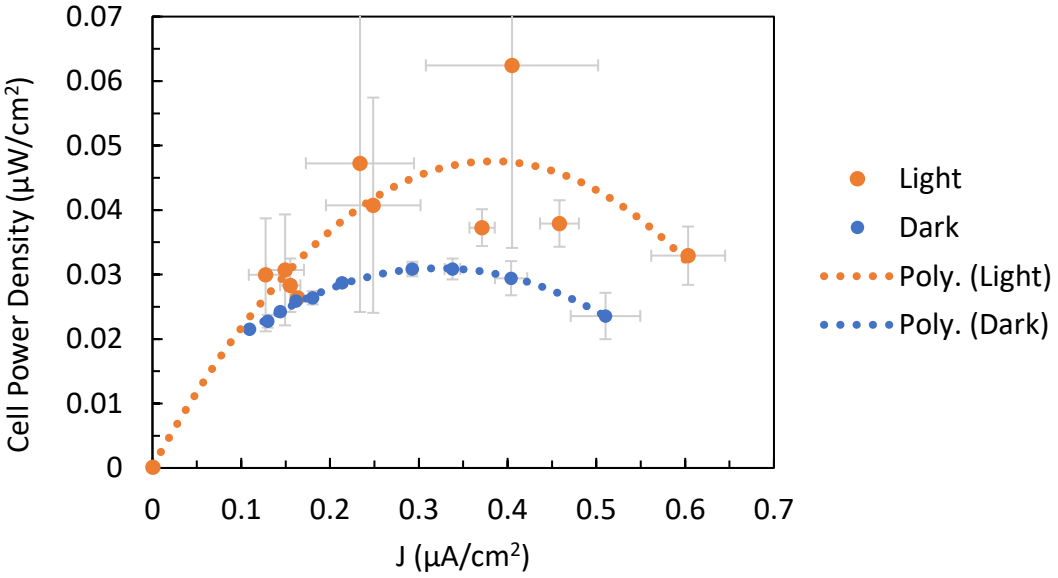

Figure 30. Cu_2O cathode power density curves under light and dark conditions.

However, after integrating the graphite felt power density curve (Figure 31) seems that the power production of photocathode is extremely low compared to graphite felt, showing a difference of 0.10 µW/cm^2. Although the catalyst shows a good performance, it enhances the activation losses, but the ohmic losses, difficult the flow of electrons in the system and therefore a low performance is displayed.

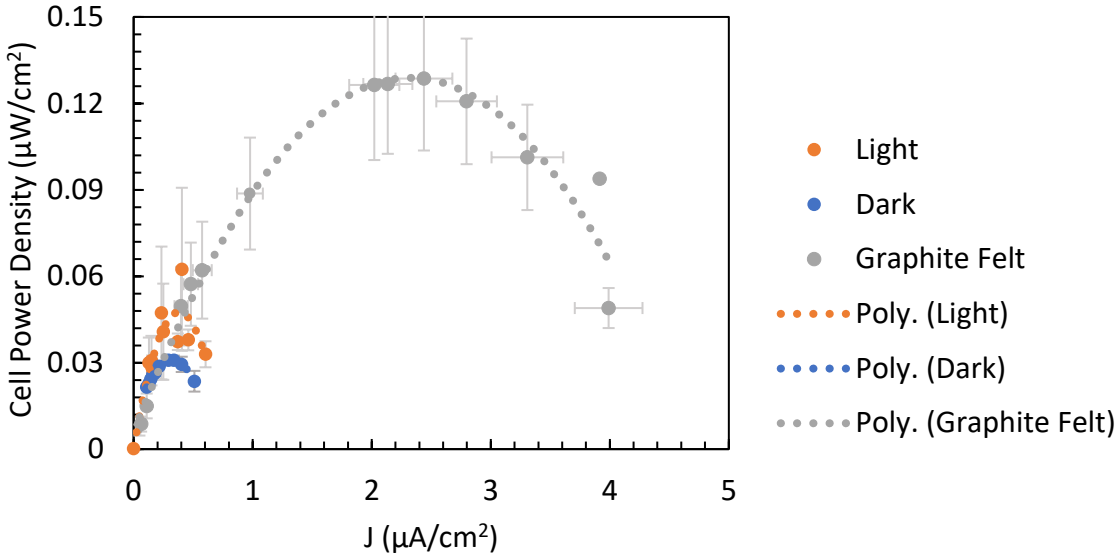

Figure 31. Cu_2O cathode vs Graphite felt cathodes power density curves comparison.

Secondly, the Cu_2O + Nafion system polarization curves, displayed in Figure 32, show a similar V_{OC} between both systems, with an approximately 25 mV difference. With the dark conditions, the curve show a small amount higher V_{OC}. However, the illuminated conditions curve increases the double of the dark conditions curve I_{SC} value. These could be attributed to the Nafion that could give uniformity in the catalytic activity of Cu_2O but in terms of current production, the Nafion layer enhanced considerably the photogenerated electron transfer to the soil.

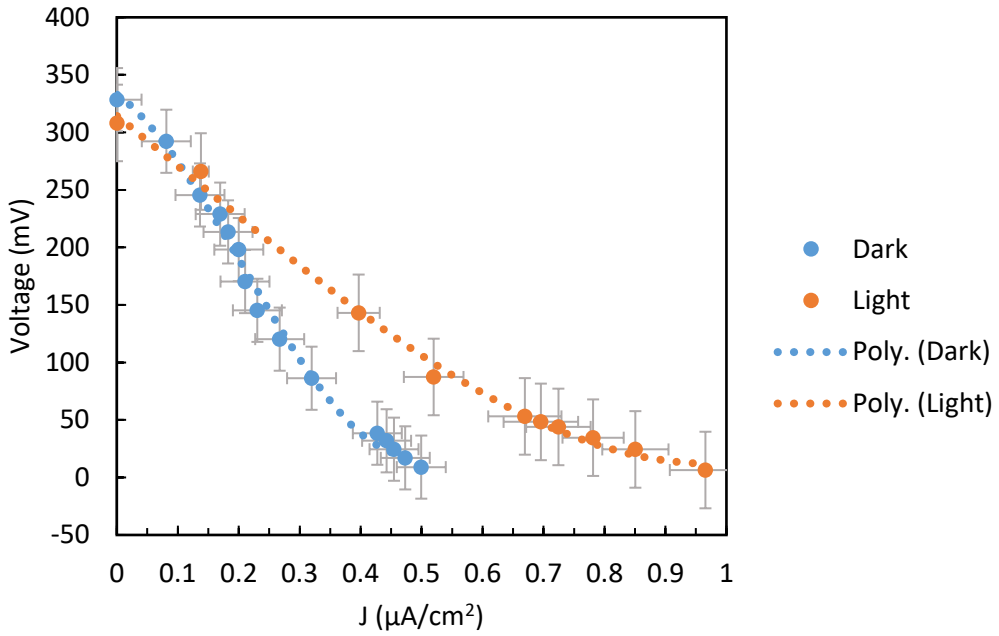

Figure 32. Cu_2O + Nafion photocathode Polarization Curve comparison in dark and light conditions.

The graphite felt comparison with photocathode polarization curves are shown in Figure 33. As it was said in the Cu_2O system, photocathodes under light and dark conditions shows a high V_{OC} compared to graphite felt which V_{OC} is even more lower than the Cu_2O system showed in Figure 29. However, the I_{SC} that the graphite felt cathode showed is almost triple. Even though the photocathode I_{SC} current is not comparable with graphite felt, is very similar (around 0.5 µA/cm^2 in dark conditions and higher in illuminated conditions compared with the Cu_2O system).

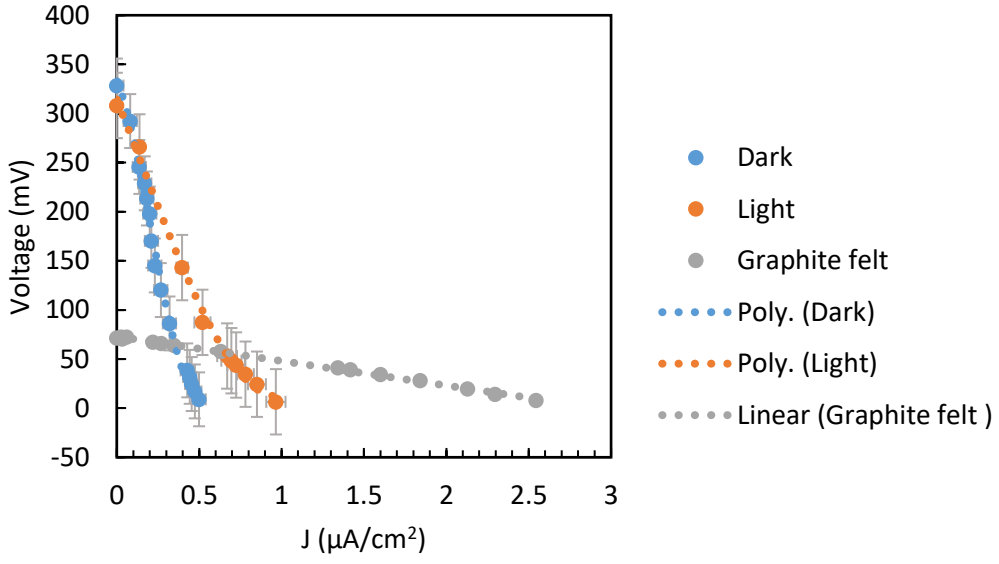

Figure 33. Cu_2O + Nafion cathode polarization curves comparison vs Graphite Felt cathode.

Due the similar early behaviour of both Cu_2O + Nafion systems, power density curves present similar shapes, see Figure 34. The power density curves exhibit a difference of 0.2 µA/cm^2 of maximum power production between light and dark conditions. Moreover, the curves present perfectly that under light conditions the current increases approximately double of the values under dark conditions. Additionally, the systems behaviour seems considerably stable compared to the Cu_2O systems. However, power production is remarkable similar between two systems but only the current production increases.

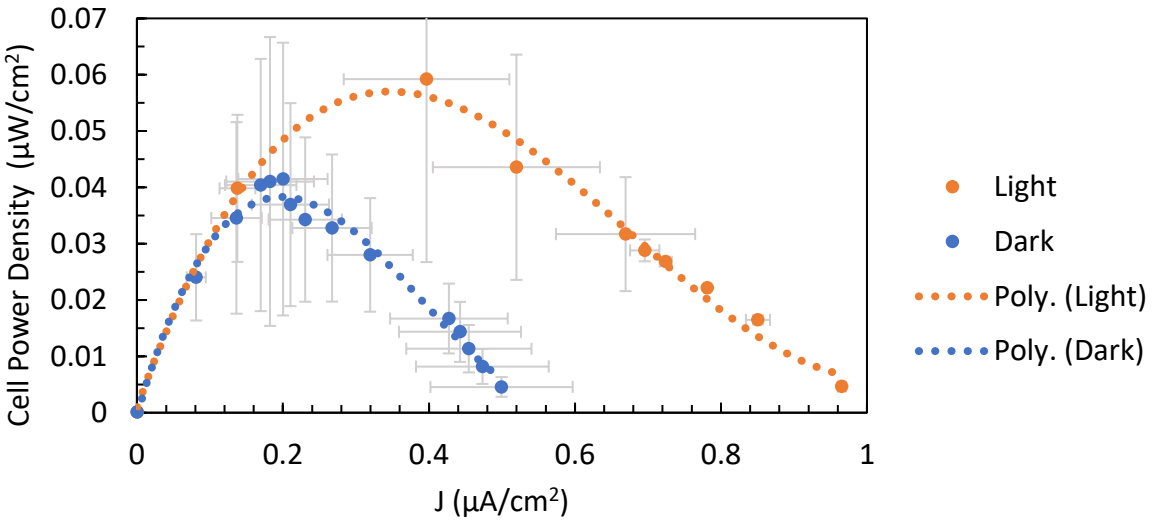

Figure 34. Cu_2O with Nafion membrane cathode power density curves under illumination and dark conditions.

In comparison with the graphite felt system, the Cu_2O + Nafion photocathode system's current production is particularly similar. As we saw in Figure 33, graphite felt system seems to have less current production activity compared with Cu_2O graphite felt systems. This is because graphite felt cathode was losing its activity over time, because the measurement protocol of each system was not carried out at the same time and for that reason as the activation losses and ohmic losses increase until achieving similar values like photocathode systems. It is important to mention that each SMFC system is different and each replacement might be compared with their graphite cathode system base where photocathode was replaced.

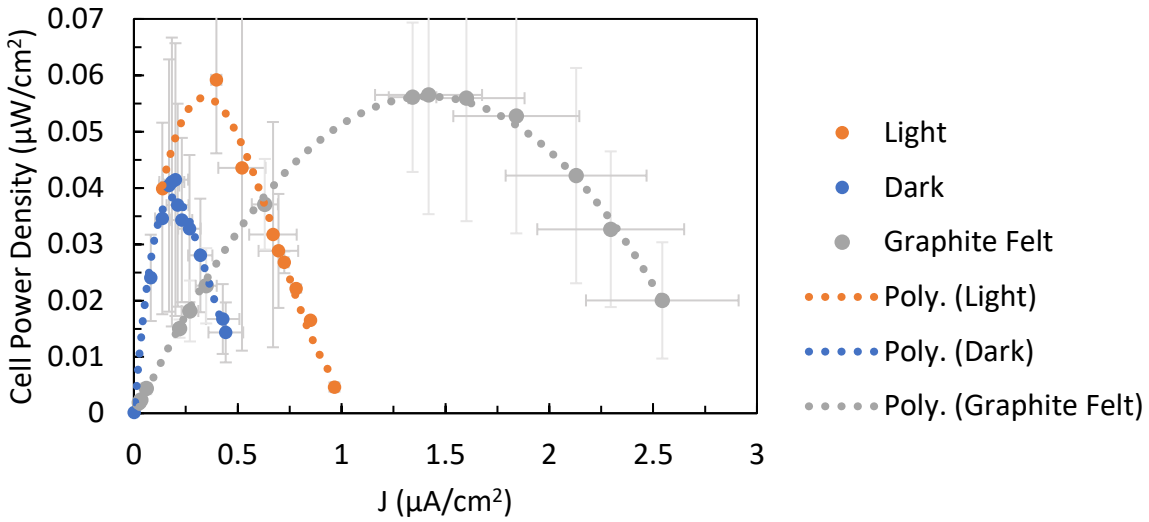

Figure 35. Comparison of Cu_2O with Nafion membrane cathode vs. Graphite felt power curves.

$LaFeO_3$ is introduced for the first time as a cathode for a microbial fuel cells, the light/dark conditions polarization curve comparison is shown in Figure 36 where the light-induced voltage is clear because the V_{OC} under light conditions is approximately 100 mV higher than the V_{OC} under dark conditions. This phenomenon is coherent with the photoelectrochemical behaviour of $LaFeO_3$, because as was presented and discussed in the Figure 22 which displays that the electron transfer starts at more positive voltages under light conditions and where under dark conditions the material's electrocatalytic activity is lower compared to Cu_2O. This condition could be illustrated comparing both current production of Cu_2O systems and $LaFeO_3$ system in the SMFC, where current production is approximately two times higher in Cu_2O systems. $LaFeO_3$ systems has a high photoactivity in terms of photo-voltage production, which it could be called light-induced overvoltage, however also present lower current productions under both light and dark conditions.

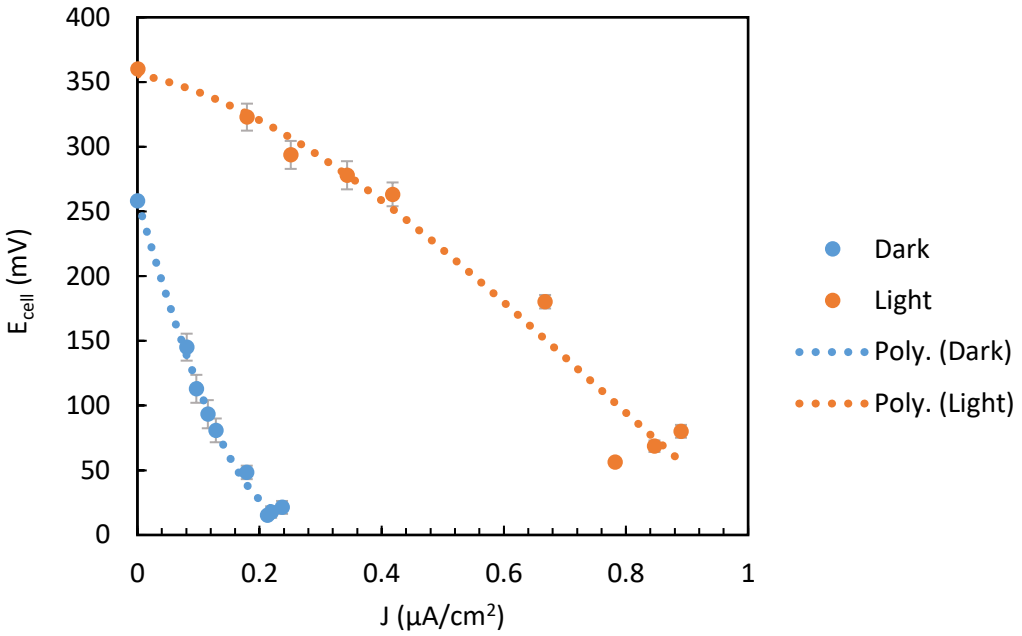

Figure 36. Comparison of $LaFeO_3$ photocathode polarization curves under dark and light conditions.

The polarization curve of graphite felt compared with $LaFeO_3$ photoelectrode system is presented in Figure 37. Graphite felt system displayed a considerably low activity, compared with the previously graphite felt systems. This can be due that these systems were the last part of the characterization protocol system and with time could degrade them. This figure displayed a low V_{OC} potential on graphite felt polarization curve, but the current production is still higher than the photocathode system which could be interpreted as the ohmic resistances in graphite felt systems are still lower even if the cathode potential is low. This system is a perfect illustration of what variables are involved in a MFC system performance and operation.

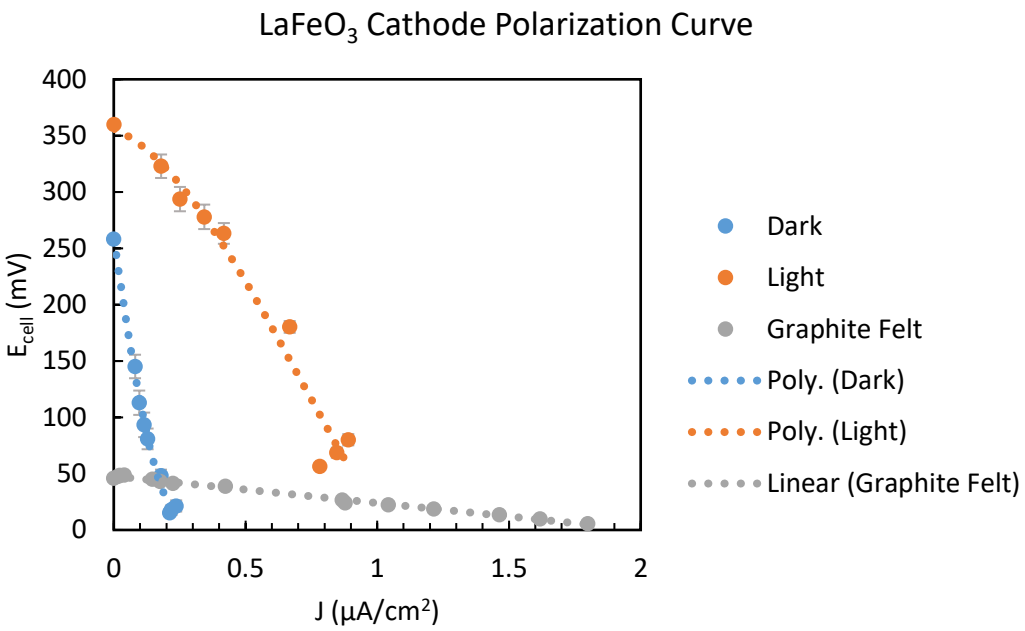

Figure 37. Comparison of $LaFeO_3$ photocathode Polarization Curve comparison in dark and light conditions vs graphite felt.

The photocathodes Power density curves are shown in Figure 38 were also illustrates the clear difference and photoactivity between dark and light conditions. The photo current and photo voltage produced under light conditions enhance the SMFC overall performance given a difference of >10 $\mu W/cm^2$ of power production and 0.8 $\mu A/cm^2$ of current production.

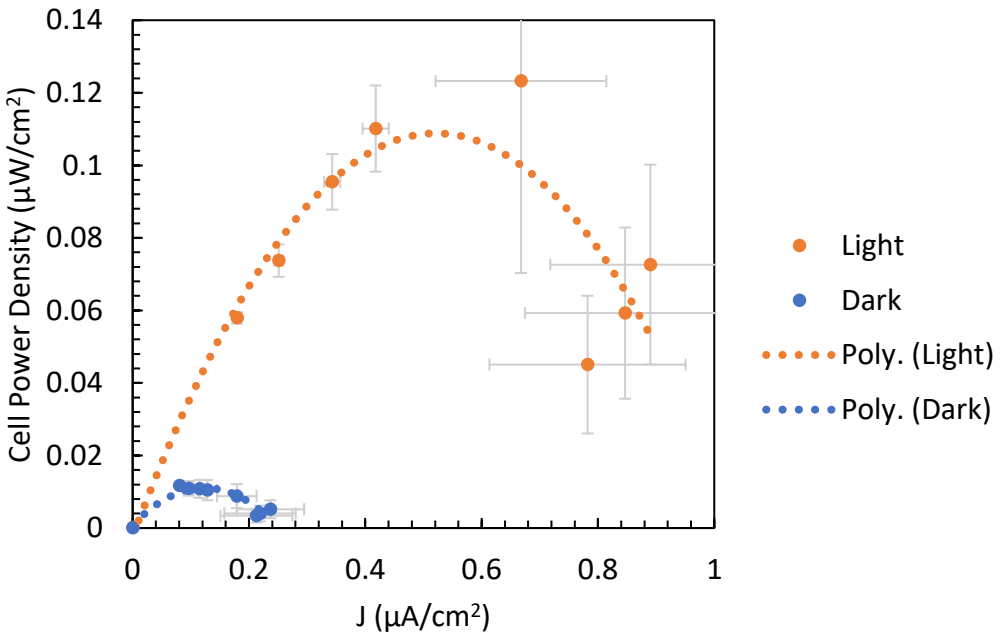

Figure 38. $LaFeO_3$ photocathode Power Density Curve comparison in dark and light conditions.

The graphite felt in comparison with photocathode power density curves shows the lower performance, but the system still has a high current density. When cathode was replaced for $LaFeO_3$ the system performance was poor due the low catalytic activity under dark conditions, but when the cathode was illuminated the system performance was envidently enhanced due of synergetic effect of a high produced photovoltage, which is the main factor of the electrocatalytic activity, and photocurrent production, which enhance the electron transfer. In general terms, $LaFeO_3$ cathode show an extremely clear photoactivity under light conditions.

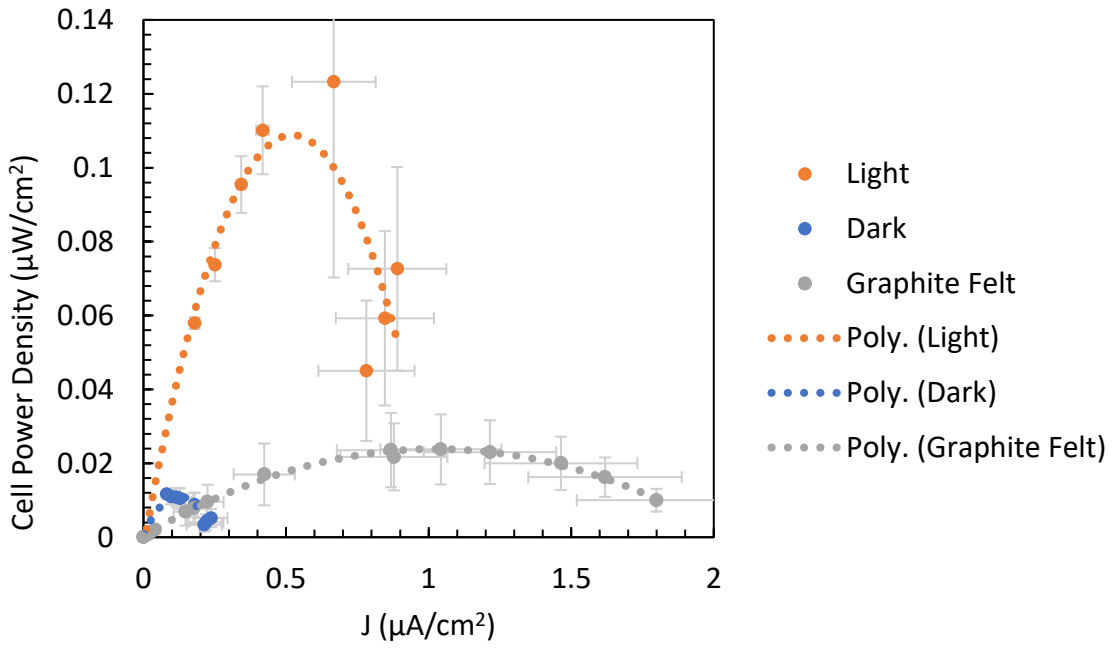

Figure 39. Comparison of $LaFeO_3$ cathode vs. Graphite felt power curves.

Figure 40 resumes the power density production comparison of each cathode system. The highest power density peak obtained value by graphite felt systems were 0.15 µW/cm^2. The power density peak difference between light and dark conditions obtained by each photocathode was 0.031 µW/cm^2, 0.017 µW/cm^2 and 0.1104 µW/cm^2 which correspond to Cu_2O, Cu_2O + Nafion and $LaFeO_3$ systems, respectively.

The Cu_2O and Cu_2O + Nafion systems have shown a similar electrocatalytic activity under both conditions in consequence a similar power density production. However Cu_2O + Nafion system shows a slightly higher power production under dark conditions, that means that Nafion layer uniforms ion transport through the cathode-soil interface, in consequence, enhance in general terms the electron transfer mechanism even under dark conditions as the Figure 40 shows.

$LaFeO_3$ photocathode system showed the highest power density production photoactivity under light conditions, due to its clearly enhanced photo-electrocatalytic activity that polarization and power density curves have shown in Figure 37 and Figure 39. Also, it is clear that the $LaFeO_3$ performance under light conditions is comparable higher than the higher Graphite Felt cathode's power density production. $LaFeO_3$ photocathode is a promising material for MFC applications because it was demonstrated that its properties under illumination creates changes in the semiconducting material properties and that influence directly the ORR thermodynamics and electron transfer characteristics.

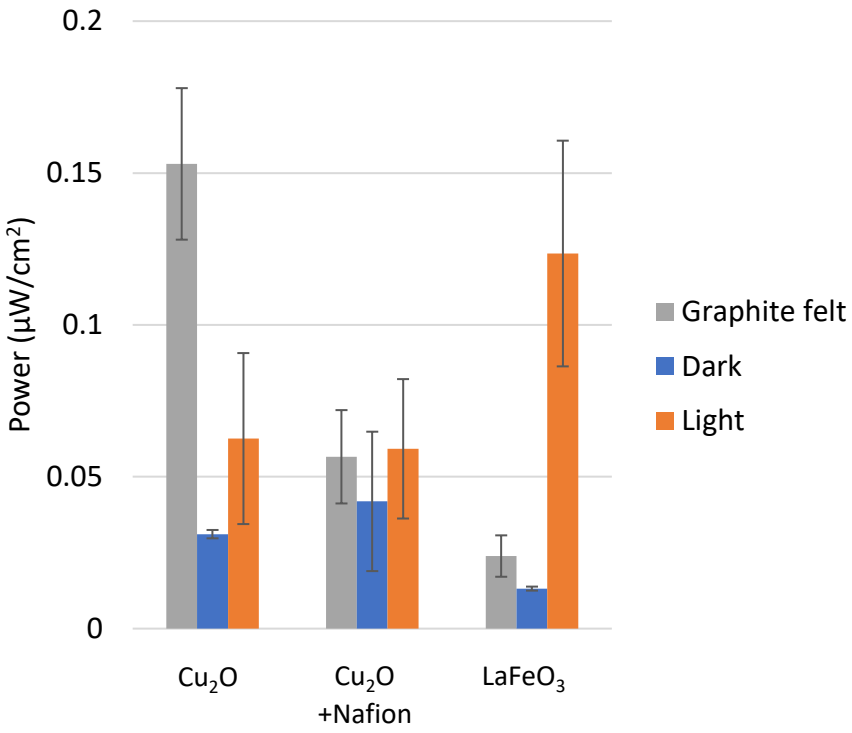

Figure 40. Comparison of average power density peak with graphite felt and under dark and light conditions.

Figure 41 resumed results of the maximum average current in each system. The maximum photocurrent production difference between dark and light conditions for the $LaFeO_3$ cathode system is more pronounced than Cu_2O and Cu_2O + Nafion, which is coherent with the previous displayed results. In case of the comparison of Cu_2O and Cu_2O + Nafion systems also presents similar current production under dark conditions, where Cu_2O + Nafion presents slightly higher current production in under illumination, this behaviour is also coherent with previous discussed results in this study and also coincident with previous studies (Castresana et al., 2019).

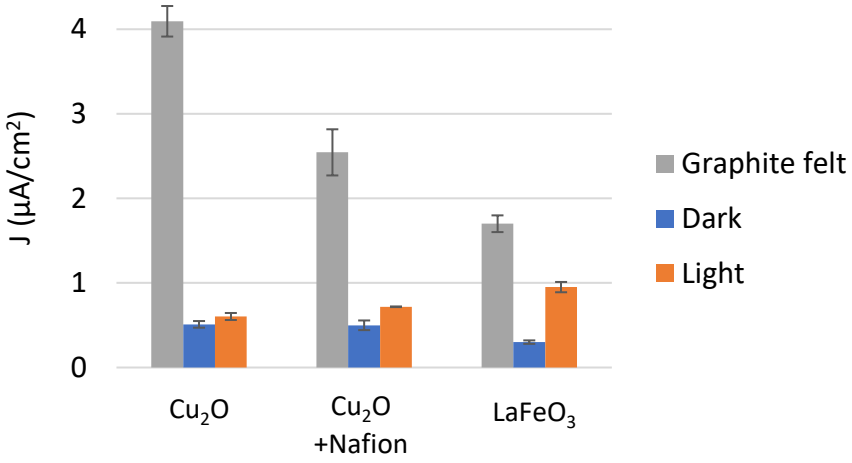

Figure 41. Comparison of average maximum current production with graphite felt and the semiconductors under dark and light conditions.

The internal resistances of the system were calculated with Equation 3.

Figure 42. shows a results resume comparing internal resistances of each systems. The considerable high internal resistances in each photocathode systems is attributed to the created resistance between soil and photocathode, also to a struggle in the connection between the wire to FTO surface of photocathodes. Nevertheless, $LaFeO_3$ has less internal resistance in comparison with the other systems, because display clear charge transfer at system level, as previous presented results showed. Although, still a high resistance. Nafion addition in Cu_2O photocathode systems shows that it notably decreases the internal resistance of the Cu_2O photocathode system slightly more than 50% compared with no Nafion membrane system.

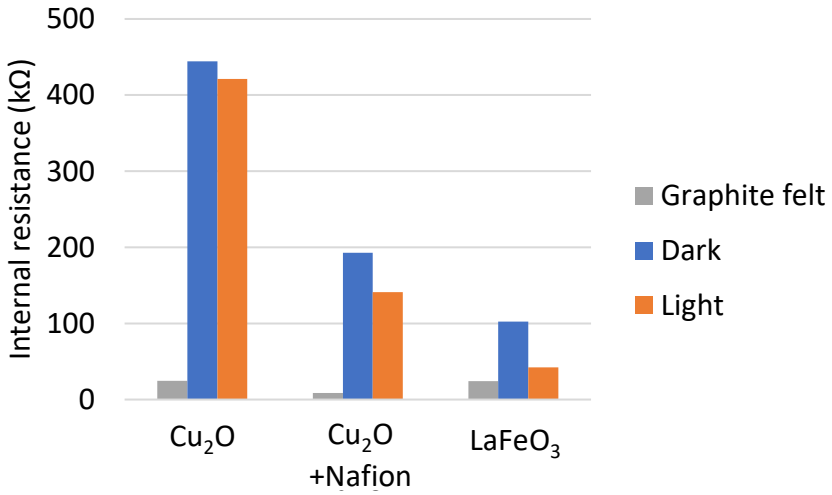

Figure 42. Comparison of the average internal resistance of the systems with graphite felt and photocathodes under dark and light conditions.

Polarization curves of each system (Figure 29,Figure 33 and Figure 37) with Cu_2O, Cu_2O + Nafion, $LaFeO_3$ and graphite felt individual electrode potential are displayed in Figure 43. The photoelectrode systems have notably low activation losses, that means that the reduction potentials at the photocathodes are high but the ohmic losses and internal resistance on the overall system are too high, which forces the bioactive bacteria at the anode to oxidize organic matter faster. As a consequence, releases more electrons and protons at the anode, which are not transformed completely at the cathode. This phenomenon causes the fast potential dropping observed in polarization curves or photocathode systems in contrast with polarization curves of graphite felt cathode systems, which have an almost linear behaviour. Also, high internal resistances in the system are attributed to this phenomenon, which are caused by ohmic losses related to the poor connection between wires and electrodes, and interfaces resistance (connections between soil and electrode).

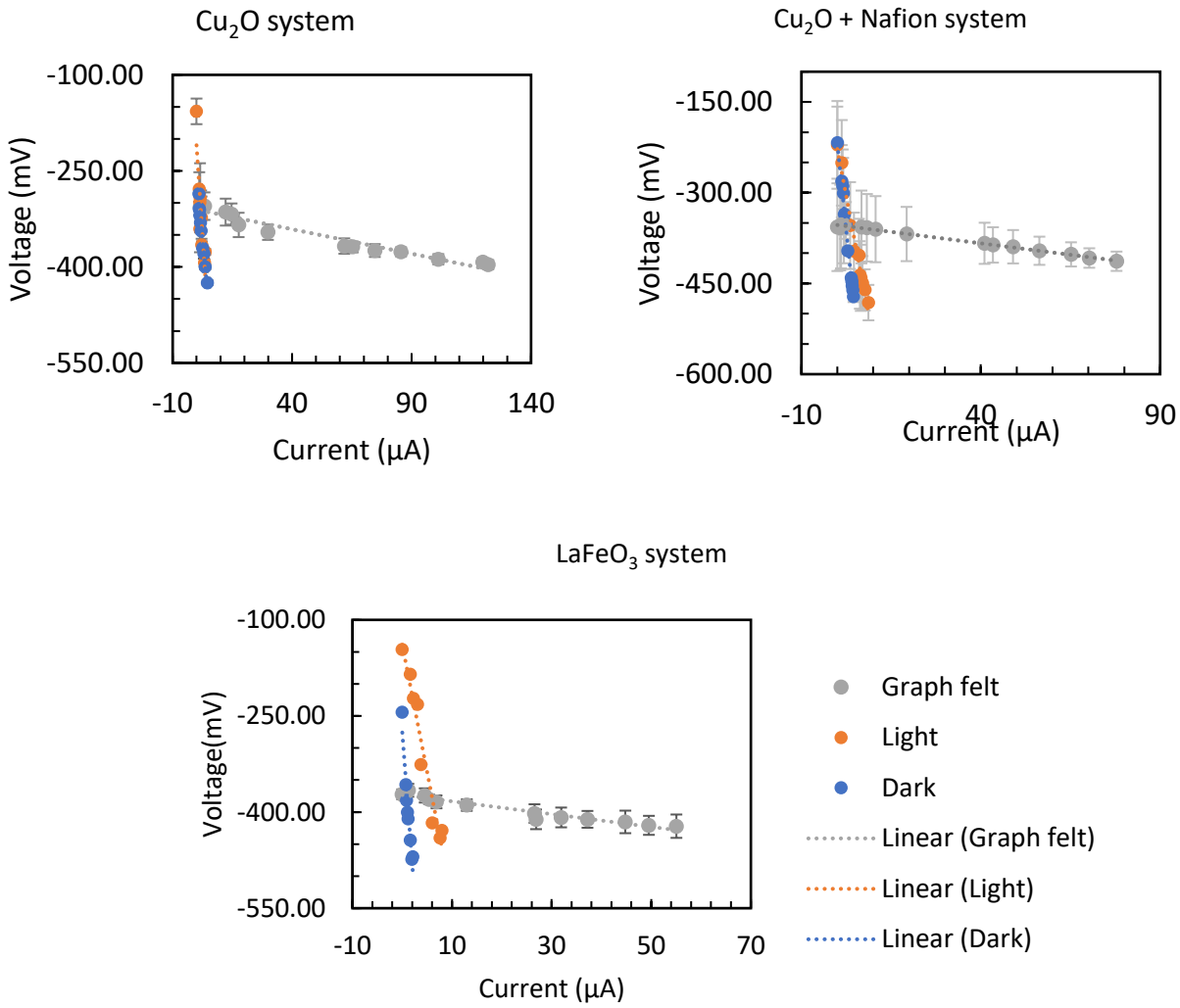

Figure 43. Individual cathode potential of each system under light and dark conditions.

As it was exposed in the Chapter 1, there are two processes to contemplate in a PMFC that they can be used to explain the differences of current generation.

1. The generation and transference of bio-generated electrons at the anode.
2. The photocurrent generation of electron/hole pairs (e^-/h^+).

For each SMFC the process efficiency is related with the anode electro active bacteria's capacity to oxidise organic matter and consequently generate electrons and protons. Then, electrons flow achieves the cathode crossing by an external circuit, while protons are diffused to reach the cathode through the soil.

In the absence of light, all cathodic materials used in each system act like conductor of bio-generated electrons. When photocathode is irradiated by light is also activated to generate e^-/h^+, as consequence a higher cathode potential respect of bio-anode is achieved, as is shown in Figure 44. Under the light-acid conditions of soil (pH = 5 or 6), the photoinduced electrons of conduction band reduce the oxygen to OH^- or H_2O near to the cathode/soil interface. While holes (h^+) on valence band are recombined with bio-generated electrons avoiding the recombination with the photoinduced electrons. The enhance the electron transfer in illuminated face is attributed to photogenerated holes (Castresana et al., 2019; S. Wang et al., 2014).

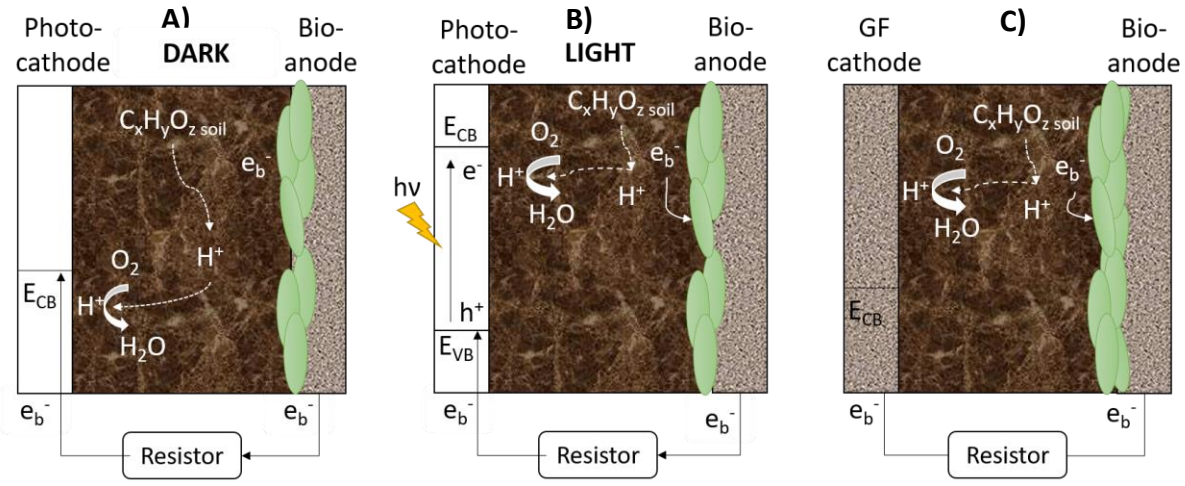

Figure 44. The diagram of charge transfer mechanism and process scheme of A) Photocathode systems under dark conditions, B) Photocathode systems under light conditions and C) graphite felt (GF) under both dark and light conditions. Adapted from (Castresana et al., 2019).

Dark and light cycles performance

After discharge test characterization, dark-light conditions cycled test was carried out. It consisted on dark and light conditions periodically applied to the photocathode systems each 6 hours

completing 3 dark-light cycles in total. A 40 kΩ external resistance was applied to each system after discharge tests with the objective to compare systems behaviour at same conditions.

The dark and light cycles' current production are showed in Figure 45, where the cycles created by light or dark conditions are evident. It is possible to observe that current production of plain Cu_2O photoelectrode decrease 0.45 µA with time due Cu_2O leaching into the solid or material photo corrosion which decrease material photoactivity and is one of the most important problems of Cu_2O. On the other hand, the current produced by Cu_2O + Nafion system is similar with Cu_2O but it shows an increasing difference of 0.21 µA at the end of the experiment. This increase is attributed to the added Nafion membrane. As time passes, more electrons are being produced at the anode; the cathode, in addition to limiting the transfer of electrons with the catholyte, is also limiting the production of electrons at the anode, which shows the constant current in the Cu_2O electrode. On the other hand, by increasing the efficiency of electron transport at the cathode, adding Nafion membrane for instance, the current produced by the system also increases over time. In contrast, $LaFeO_3$ cathode showed the same cyclic behaviour. But even if the current production is notably lower, due the high applied external resistance (40 kΩ) which is notably higher than the internal resistance of the system that was previously calculated (Figure 42. Comparison of the average internal resistance of the systems with graphite felt and photocathodes under dark and light conditions.) (Dziegielowski, 2018). The $LaFeO_3$ cathode presents a considerably stable current production compared to Cu_2O-based systems. The high current production peak observed in $LaFeO_3$ timeline is attributed to recombination of the charge's separation (e^-/h^+) and the immediately recombination of them.

In conclusion, each photocathode increases cathode potential in the system. However, current and power production in the systems are still very low compared with other published works. Also, the constructed systems had a connection issue when the photocathode was replaced and took place in the system. It could be between many interfaces: soil-photocathode interface, external circuit wire and photocathode conductive surface etc. Another limiting factor is photocathode area that compared with graphite felt cathode that its active surface is larger (30.9 cm^2 vs 9 cm^2 of photocathode geometric area), it means that the electron flows better in graphite felt cathode. However, the photocathodes were demonstrating that they are more catalytic powerful than graphite felt, showing a good and more positive cathode potential using a relative low amount of material compared with graphite felt. It is necessary to focus to enhance the connections between interfaces in the system, especially, photocathode and external circuit connection and increasing electrolyte conductivity (soil conductivity).

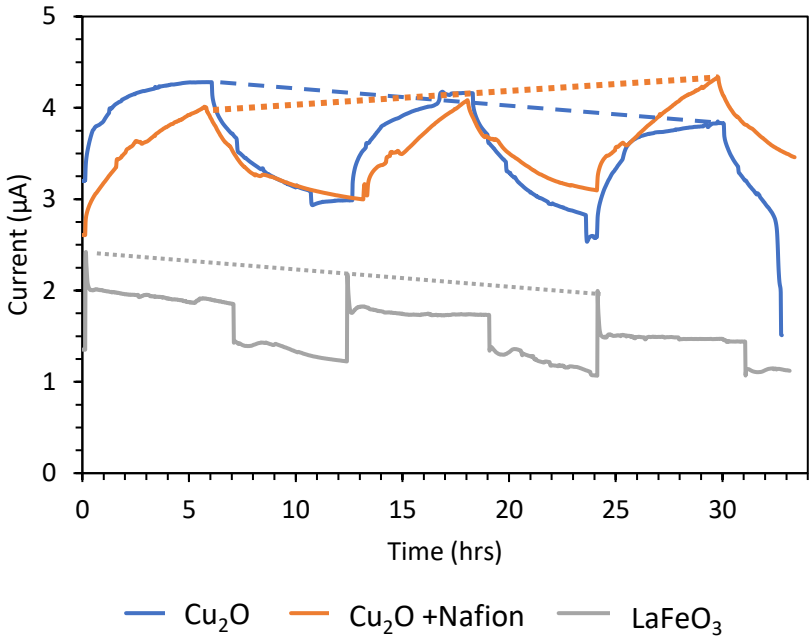

Figure 45. Evolution of the current production with time for the six systems. Each system has an internal resistance of 40 kΩ.

Chapter 4 - Conclusions and further research

The main goal of this thesis project work was to enhance the cathode performance in a Soil Microbial Fuel Cell operation. In order to achieve this objective three cathode arrays of photoactive materials were proposed and synthesised, characterised and then implemented in a Soil Microbial Fuel Cell which performance was evaluated. The main findings are enumerated below:

Photocathode materials:

1) Tetrahedral shaped Cu_2O nanoparticles were successfully synthesized via solvothermal method. The nanoparticles have shown a maximum of 1.97 mA/cm^2 of photocurrent production in PEC measurements. They also displayed (111) plane as a predominant crystallographical plane which was related to the high photocurrent production of Cu_2O in previously studies because it increases the active surface area which is in contact with the electrolyte and material electrons. The (111) crystal plane is also related to building the tetrahedral shape which optical and SEM characterization showed. Even this synthesis method is apparently cheap and straightfoward, it would be necessary for the photo-electrochemistry technology development to search sustainable and green methods of synthesis to reduce the environmental impact for scale up the technology.
2) Uniform $LaFeO_3$ thin films with a perovskite structure was synthesized via polymeric template spin coating method. $LaFeO_3$ show an earlier photovoltage production and electron transfer at more positive potentials. This is a relevant property of $LaFeO_3$ for photo-electrocatalytic performances because under radiated conditions, the energy required to carry out a reduction reaction is reduced which is the objective of electrocatalyst materials. However, $LaFeO_3$ also shows a lower photocurrent compared with Cu_2O. Further research is necessary to explore physicochemical properties with material simulation and understand how photovoltage and photocurrent are produced and how influences the electrocatalytic activity in several conditions.
3) $LaFeO_3$ was tested to see its ORR activity under neutral and alkaline pH conditions. The results corroborate that the $LaFeO_3$ could have photoelectroactivity and an earlier electron transfer on ORR activity which confirm that this material can be used for SMFC conditions.
4) The materials showed photoactivity when they were irradiated with a LED lamp which was similar that the one used in the main experiment. However, the photocurrent produced when irradiated with a LED lamp is considerably lower due to lamp intensity. Nevertheless, the

produced photocurrent was enough to observe a change between dark and light conditions. Lamp spectra is important for the optimal photoactivity of semiconductors, it would be necessary to use a lamp which its spectra will be aligned with the material absorption spectra. Moreover, one of the main goals of this technology is using this under the presence of sunlight. For that reason, sunlight conditions studies are required.

5) Photocathode Area experiment showed that a single large surface electrode has a better photoactive performance than same-area small electrodes array due the reduction of small ohmic losses which array connections are produced. However, exploring the relation of photocathode area and its effect on microbial fuel cell efficiency is necessary for system scale up. It is important to consider the change in photoelectroactivity when the surface area increase. On the other hand, an investigation of material synthesis scale up it would be necessary.
6) The Nafion layer addition of the Cu_2O surface shows an evident increase in current production because of its uniformity on the transport phenomena and clearly enhance the electron transfer and ORR electrocatalysis. This first exploration research opens up new opportunities to understand how the effect of Nafion layer on photo-electrocatalytic properties is carried out, photo-electron transport mechanism and the stability of photogenerated carriers. This is a relevant research line because it could be applied in both Fuel Cells and biological fuel cells.

Soil Microbial Fuel Cells Systems implemented with photocathode:

7) The soil microbial fuel cell was perfectly set up and the grown period shows the three main phases of biofilm growth period until a pseudo-stability state after three weeks (21 days) of operation. Results also show that individual electrode potential changed: anode reached more negative potentials and cathode reach more positive potentials. The described behaviour shows that a biofilm was formed in SMFC systems. Previous studies have shown that SMFC could have a better biofilm performance and stability if the growth period is larger.
8) Discharge test results have produced polarization curves and power density curves. Polarization test showed that when photocathodes replacement was made, the V_{OC} was higher than graphite felt. Cu_2O-based systems showed a similar V_{OC} increase, however, Cu_2O + Nafion system present double higher I_{SC} values and slightly higher under light conditions. In $LaFeO_3$, both V_{OC} and I_{SC} increment between dark and light conditions was very evident, positioning $LaFeO_3$ as the materials that presents best photo-response results at SMFC systems level.

9) Power curves comparison shows that the Cu_2O-based system has a similar power output and Nafion membranes enhance power production in even in dark conditions. On the other hand, $LaFeO_3$ presents the three constructed SMFC system's highest power output under illuminated conditions due its photo-electroactivity.
10) Comparing this work with previously results, the obtained results present a low power output due higher internal resistance in the systems. For that reason, future studies must put more attention on both systems potentially ohmic losses especially on electrode-wire connections and electrolyte conductivity. It will be interesting to explore the electrolyte conductivity property on the power output and its biocompatibility.

Wider significance of research

This study demonstrates that implementation of photoactive materials as cathode in Soil Microbial Fuel Cells or in BES systems can produce an important enhancement on the systems power output performance. Overcoming electrochemical losses is the most important challenge in BES to technology commercialization. The soil microbial fuel cells technology can derive different potential applications like, decentralized power generation systems, Plant-Microbial Fuel Cell systems, bioremediation systems, and biosensors etc.

Bibliography

Ampudia, P., Monasterio, S., Freeman, E., Eslava, S., & Di, M. (2019). Electrochimica Acta Electricity generation from moss with light-driven microbial fuel cells. *Electrochimica Acta*, *298*, 934–942. https://doi.org/10.1016/j.electacta.2018.12.108

Bhowmick, G. D., Noori, M. T., Das, I., Neethu, B., Ghangrekar, M. M., & Mitra, A. (2018). Bismuth doped TiO2 as an excellent photocathode catalyst to enhance the performance of microbial fuel cell. *International Journal of Hydrogen Energy*, *43*(15), 7501–7510. https://doi.org/10.1016/j.ijhydene.2018.02.188

Borja-Arco, E., Sandoval, O. J., Escalante-García, J., Sandoval-González, A., & Sebastian, P. J. (2011). Microwave assisted synthesis of ruthenium electrocatalysts for oxygen reduction reaction in the presence and absence of aqueous methanol. *International Journal of Hydrogen Energy*, *36*(1), 103–110. https://doi.org/10.1016/j.ijhydene.2010.10.051

Castresana, P. A., Martinez, S. M., Freeman, E., Eslava, S., & Di Lorenzo, M. (2019). Electricity generation from moss with light-driven microbial fuel cells. *Electrochimica Acta*, *298*, 934–942. https://doi.org/10.1016/j.electacta.2018.12.108

Chen, Q. Y., Liu, J. S., Liu, Y., & Wang, Y. H. (2013). Hydrogen production on TiO2 nanorod arrays cathode coupling with bio-anode with additional electricity generation. *Journal of Power Sources*, *238*, 345–349. https://doi.org/10.1016/j.jpowsour.2013.04.066

Cullity, B. D. (1978). *Elements of X-ray Diffraction*. Addison-Wesley Publishing Company. https://books.google.com.mx/books?id=WpxpAAAAMAAJ

Díez-García, M. I., & Gómez, R. (2017). Metal Doping to Enhance the Photoelectrochemical Behavior of LaFeO(3) Photocathodes. *ChemSusChem*, *10*(11), 2457–2463. https://doi.org/10.1002/cssc.201700166

Ding, H., Li, Y., Lu, A., Jin, S., Quan, C., Wang, C., Wang, X., Zeng, C., & Yan, Y. (2010). Photocatalytically improved azo dye reduction in a microbial fuel cell with rutile-cathode. *Bioresource Technology*, *101*(10), 3500–3505. https://doi.org/10.1016/j.biortech.2009.11.107

Dziegielowski, J. (2018). *Plant Microbial Fuel Cells : Design Optimization & Scale-up*.

Fischer, F. (2018). Photoelectrode, photovoltaic and photosynthetic microbial fuel cells. *Renewable and Sustainable Energy Reviews*, *90*(June 2017), 16–27.

https://doi.org/10.1016/j.rser.2018.03.053

Freeman, E., Kumar, S., Celorrio, V., Park, M. S., Kim, J. H., Fermin, D. J., & Eslava, S. (2020). Strategies for the deposition of LaFeO3 photocathodes: Improving the photocurrent with a polymer template. *Sustainable Energy and Fuels*, *4*(2), 884–894. https://doi.org/10.1039/c9se01103j

Fujishima, A., & Honda, K. (1972). Electrochemical Photolysis of Water at a Semiconductor Electrode. *Nature*, *238*(5358), 37–38. https://doi.org/10.1038/238037a0

Gul, M. M., & Ahmad, K. S. (2019). Bioelectrochemical systems: Sustainable bio-energy powerhouses. *Biosensors and Bioelectronics*, *142*(July). https://doi.org/10.1016/j.bios.2019.111576

Guo, D., Song, R. Bin, Shao, H. H., Zhang, J. R., & Zhu, J. J. (2017). Visible-light-enhanced power generation in microbial fuel cells coupling with 3D nitrogen-doped graphene. *Chemical Communications*, *53*(72), 9967–9970. https://doi.org/10.1039/c7cc04666a

Guo, D., Wei, H. F., Yu, X. Y., Xia, Q., Chen, Z., Zhang, J. R., Song, R. Bin, & Zhu, J. J. (2019). Plasmon-enhanced cathodic reduction for accelerating electricity generation in visible-light-assisted microbial fuel cells. *Nano Energy*, *57*(December 2018), 94–100. https://doi.org/10.1016/j.nanoen.2018.12.043

Han, H. X., Shi, C., Yuan, L., & Sheng, G. P. (2017). Enhancement of methyl orange degradation and power generation in a photoelectrocatalytic microbial fuel cell. *Applied Energy*, *204*, 382–389. https://doi.org/10.1016/j.apenergy.2017.07.032

Han, H. X., Shi, C., Zhang, N., Yuan, L., & Sheng, G. P. (2018). Visible-light-enhanced Cr(VI) reduction at Pd-decorated silicon nanowire photocathode in photoelectrocatalytic microbial fuel cell. *Science of the Total Environment*, *639*, 1512–1519. https://doi.org/10.1016/j.scitotenv.2018.05.271

Hankin, A., Bedoya-Lora, F. E., Ong, C. K., Alexander, J. C., Petter, F., & Kelsall, G. H. (2017). From millimetres to metres: The critical role of current density distributions in photo-electrochemical reactor design. *Energy and Environmental Science*, *10*(1), 346–360. https://doi.org/10.1039/c6ee03036j

Harnisch, F., & Rabaey, K. (2015). Bioelectrochemical Systems. In *Materials for Low-Temperature Fuel Cells*. https://doi.org/10.1002/9783527644308.ch08

IEA. (2019). *World Energy Outlook 2019*. OECD. https://doi.org/10.1787/caf32f3b-en

Jia, Y., Zhang, D., You, H., Li, W., & Jiang, K. (2019). Benthic microbial fuel cell equipped with a photocatalytic Cu 2 O-coated cathode. *Journal of Nanoparticle Research*, *21*(1). https://doi.org/10.1007/s11051-018-4444-7

Jiang, C., Liu, L., & Crittenden, J. C. (2016). An electrochemical process that uses an Fe0/TiO2 cathode to degrade typical dyes and antibiotics and a bio-anode that produces electricity. *Frontiers of Environmental Science and Engineering*, *10*(4), 1–8. https://doi.org/10.1007/s11783-016-0860-z

Larminie, J., Dicks, A., Larminie, J., & Dicks, A. (2013). Efficiency and Open Circuit Voltage. In *Fuel Cell Systems Explained*. https://doi.org/10.1002/9781118878330.ch2

Li, X., Liu, D., Mo, X., & Li, K. (2019). Nanorod β-Ga2O3 semiconductor modified activated carbon as catalyst for improving power generation of microbial fuel cell. *Journal of Solid State Electrochemistry*, *23*(10), 2843–2852. https://doi.org/10.1007/s10008-019-04377-4

Li, Yan, Lu, A., Ding, H., Jin, S., Yan, Y., Wang, C., Zen, C., & Wang, X. (2009). Cr(VI) reduction at rutile-catalyzed cathode in microbial fuel cells. *Electrochemistry Communications*, *11*(7), 1496–1499. https://doi.org/10.1016/j.elecom.2009.05.039

Li, Yihua, Sun, J., Liu, L., & Yang, F. (2017a). A composite cathode membrane with CoFe2O4-rGO/PVDF on carbon fiber cloth: synthesis and performance in a photocatalysis-assisted MFC-MBR system. *Environmental Science: Nano*, *4*(2), 335–345. https://doi.org/10.1039/c6en00454g

Li, Yihua, Sun, J., Liu, L., & Yang, F. (2017b). A composite cathode membrane with CoFe2O4-rGO/PVDF on carbon fiber cloth: synthesis and performance in a photocatalysis-assisted MFC-MBR system. *Environmental Science: Nano*, *4*(2), 335–345. https://doi.org/10.1039/c6en00454g

Logan, B. (2008). *Microbial Fuel Cells*. https://doi.org/DOI: 10.1016/B978-0-444-53199-5.00098-1

Logan, B. E. (2008). *Microbial Fuel Cells*.

Logan, B. E., Hamelers, B., Rozendal, R., Schröder, U., Keller, J., Freguia, S., Aelterman, P., Verstraete, W., & Rabaey, K. (2006). Microbial fuel cells: Methodology and technology. *Environmental Science and Technology*, *40*(17), 5181–5192. https://doi.org/10.1021/es0605016

Long, X., Pan, Q., Wang, C., Wang, H., Li, H., & Li, X. (2017). Microbial fuel cell-photoelectrocatalytic cell combined system for the removal of azo dye wastewater. *Bioresource Technology*, *244*, 182–191. https://doi.org/10.1016/j.biortech.2017.07.088

Lu, A., Li, Y., Jin, S., Ding, H., Zeng, C., Wang, X., & Wang, C. (2010). Microbial fuel cell equipped with a photocatalytic rutile-coated cathode. *Energy and Fuels*, *24*(2), 1184–1190. https://doi.org/10.1021/ef901053j

M. A. Khan, M. U. T. I. H. M. A. A. K. M. S. A. M. A. A. N. A. K. (2015). Surfactant Assisted Synthesis of Cuprous Oxide (Cu2O) Nanoparticles via Solvothermal Process. *Nanoscience and Nanotechnology Research*, *3*(1), 16–22. https://doi.org/DOI:10.12691/nnr-3-1-3

Mauritz, K. A., & Moore, R. B. (2004). State of Understanding of Nafion. *Chemical Reviews*, *104*(10), 4535–4586. https://doi.org/10.1021/cr0207123

Muller, H. (2007). *PHOS-User-Manual REV4*. https://doi.org/10.13140/RG.2.2.24339.43044

Nordin, N., Ho, L. N., Ong, S. A., Ibrahim, A. H., Wong, Y. S., Lee, S. L., Oon, Y. S., & Oon, Y. L. (2017). Hybrid system of photocatalytic fuel cell and Fenton process for electricity generation and degradation of Reactive Black 5. *Separation and Purification Technology*, *177*, 135–141. https://doi.org/10.1016/j.seppur.2016.12.030

Palanisamy, G., Jung, H. Y., Sadhasivam, T., Kurkuri, M. D., Kim, S. C., & Roh, S. H. (2019). A comprehensive review on microbial fuel cell technologies: Processes, utilization, and advanced developments in electrodes and membranes. *Journal of Cleaner Production*, *221*, 598–621. https://doi.org/10.1016/j.jclepro.2019.02.172

Paracchino, A., Laporte, V., Sivula, K., Grätzel, M., & Thimsen, E. (2011). Highly active oxide photocathode for photoelectrochemical water reduction. *Nature Materials*, *10*(6), 456–461. https://doi.org/10.1038/nmat3017

Potter, M. C. (1915). Electrical effects accompanying the decomposition of organic compounds. II. Ionisation of the gases produced during fermetantion. *Proc. R. Soc. Lond.*, 465–480. https://doi.org/https://doi.org/10.1098/rspa.1915.0038

Rismani-Yazdi, H., Carver, S. M., Christy, A. D., & Tuovinen, O. H. (2008). Cathodic limitations in microbial fuel cells: An overview. *Journal of Power Sources*, *180*(2), 683–694. https://doi.org/10.1016/j.jpowsour.2008.02.074

Schreier, M., Gao, P., Mayer, M. T., Luo, J., Moehl, T., Nazeeruddin, M. K., Tilley, S. D., & Grätzel, M. (2015). Efficient and selective carbon dioxide reduction on low cost protected Cu2O photocathodes using a molecular catalyst. *Energy and Environmental Science*, *8*(3), 855–861. https://doi.org/10.1039/c4ee03454f

Su, Y., Li, H., Ma, H., Robertson, J., & Nathan, A. (2017). Controlling Surface Termination and Facet

Orientation in Cu2O Nanoparticles for High Photocatalytic Activity: A Combined Experimental and Density Functional Theory Study. *ACS Applied Materials and Interfaces*, *9*(9), 8100–8106. https://doi.org/10.1021/acsami.6b15648

Sun, Z., Cao, R., Huang, M., Chen, D., Zheng, W., & Lin, L. (2015). Effect of light irradiation on the photoelectricity performance of microbial fuel cell with a copper oxide nanowire photocathode. *Journal of Photochemistry and Photobiology A: Chemistry*, *300*, 38–43. https://doi.org/10.1016/j.jphotochem.2014.12.003

Sustainable Development Goals. (2020). https://www.undp.org/content/undp/en/home/sustainable-development-goals.html

Tahir, M. B. (2019). Microbial photoelectrochemical cell for improved hydrogen evolution using nickel ferrite incorporated WO3 under visible light irradiation. *International Journal of Hydrogen Energy*, *44*(32), 17316–17322. https://doi.org/10.1016/j.ijhydene.2019.01.067

Thirumalairajan, S., Girija, K., Mastelaro, V. R., & Ponpandian, N. (2015). Investigation on magnetic and electric properties of morphologically different perovskite LaFeO3 nanostructures. *Journal of Materials Science: Materials in Electronics*, *26*(11), 8652–8662. https://doi.org/10.1007/s10854-015-3540-z

Touach, N., Ortiz-Martínez, V. M., Salar-García, M. J., Benzaouak, A., Hernández-Fernández, F., P. de Ríos, A., El Mahi, M., & Lotfi, E. M. (2017). On the use of ferroelectric material LiNbO3 as novel photocatalyst in wastewater-fed microbial fuel cells. *Particuology*, *34*, 147–155. https://doi.org/10.1016/j.partic.2017.02.006

Venkata Mohan, S., Velvizhi, G., Annie Modestra, J., & Srikanth, S. (2014). Microbial fuel cell: Critical factors regulating bio-catalyzed electrochemical process and recent advancements. *Renewable and Sustainable Energy Reviews*, *40*, 779–797. https://doi.org/10.1016/j.rser.2014.07.109

Wan, L. L., Li, X. J., Zang, G. L., Wang, X., Zhang, Y. Y., & Zhou, Q. X. (2015). A solar assisted microbial electrolysis cell for hydrogen production driven by a microbial fuel cell. *RSC Advances*, *5*(100), 82276–82281. https://doi.org/10.1039/c5ra16919d

Wang, L., Liu, L., & Yang, F. (2018). Efficient gas phase VOC removal and electricity generation in an integrated bio-photo-electro-catalytic reactor with bio-anode and TiO 2 photo-electro-catalytic air cathode. *Bioresource Technology*, *270*(July), 554–561. https://doi.org/10.1016/j.biortech.2018.09.041

Wang, S., Yang, X., Zhu, Y., Su, Y., & Li, C. (2014). Solar-assisted dual chamber microbial fuel cell with

a CuInS2 photocathode. *RSC Advances*, *4*(45), 23790–23796. https://doi.org/10.1039/c4ra02488e

Wu, J. C., Yan, W. M., Wang, C. T., Wang, C. H., Pai, Y. H., Wang, K. C., Chen, Y. M., Lan, T. H., & Thangavel, S. (2018). Treatment of oily wastewater by the optimization of Fe2O3 calcination temperatures in innovative bio-electron-Fenton microbial fuel cells. *Energies*, *11*(3), 1–11. https://doi.org/10.3390/en11030565

Zabaniotou, A. (2018). Redesigning a bioenergy sector in EU in the transition to circular waste-based Bioeconomy-A multidisciplinary review. *Journal of Cleaner Production*, *177*, 197–206. https://doi.org/10.1016/j.jclepro.2017.12.172

Zeng, L., Li, X., Zhao, Q., Fan, S., Zhang, M., Yin, Z., & Chen, A. (2019). Boosting interfacial charge transfer and electricity generation for levofloxacin elimination in a self-driven bio-driven photoelectrocatalytic system. *Nanoscale*, *11*(45), 22042–22053. https://doi.org/10.1039/c9nr05520g

Zhang, J., Tian, B., Wang, L., Xing, M., & Lei, J. (2018). *Mechanism of Photocatalysis*. https://doi.org/10.1007/978-981-13-2113-9_1